energies

MDPI

Review

Progress towards High-Efficiency and Stable Tin-Based Perovskite Solar Cells

Syed Afaq Ali Shah [1], Muhammad Hassan Sayyad [2], Karim Khan [1], Kai Guo [3], Fei Shen [1], Jinghua Sun [1], Ayesha Khan Tareen [1], Yubin Gong [4] and Zhongyi Guo [1,3,*]

1 School of Electrical Engineering & Intelligentizaion, Dongguan University of Technology, Dongguan 523808, China; Ali.shah82@hotmail.com (S.A.A.S.); karim_khan_niazi@yahoo.com (K.K.); shenfei@hfut.edu.cn (F.S.); sunjh@dgut.edu.cn (J.S.); chemistayesha@yahoo.com (A.K.T.)

2 Faculty of Engineering Sciences, Ghulam Ishaq Khan Institute of Engineering Sciences and Technology, Topi, District Swabi, Khyber Pakhtunkhwa 23640, Pakistan; sayyad@giki.edu.pk

3 School of Computer and Information, Hefei University of Technology, Hefei 230009, China; kai.guo@hfut.edu.cn

4 National Key Lab on Vacuum Electronics, University of Electronic Science and Technology of China (UESTC), Chengdu 610054, China; ybgong@uestc.edu.cn

* Correspondence: guozhongyi@hfut.edu.cn; Tel.: +86-186-5515-1981

Received: 3 September 2020; Accepted: 29 September 2020; Published: 29 September 2020

Abstract: Since its invention in 2009, Perovskite solar cells (PSCs) has attracted great attention because of its low cost, numerous options of efficiency enhancement, ease of manufacturing and high-performance. Within a short span of time, the PSC has already outperformed thin-film and multicrystalline silicon solar cells. A current certified efficiency of 25.2% demonstrates that it has the potential to replace its forerunner generations. However, to commercialize PSCs, some problems need to be addressed. The toxic nature of lead which is the major component of light absorbing layer, and inherited stability issues of fabricated devices are the major hurdles in the industrialization of this technology. Therefore, new researching areas focus on the lead-free metal halide perovskites with analogous optical and photovoltaic performances. Tin being nontoxic and as one of group IV(A) elements, is considered as the most suitable alternate for lead because of their similarities in chemical properties. Efficiencies exceeding 13% have been recorded using Tin halide perovskite based devices. This review summarizes progress made so far in this field, mainly focusing on the stability and photovoltaic performances. Role of different cations and their composition on device performances and stability have been involved and discussed. With a considerable room for enhancement of both efficiency and device stability, different optimized strategies reported so far have also been presented. Finally, the future developing trends and prospects of the PSCs are analyzed and forecasted.

Keywords: Perovskite Solar Cells (PSCs); lead free; nanomaterial; photovoltaic; renewable energy

1. Introduction

For the ever-growing global energy consumption and rapidly depleting fossil fuels reserves, production of energy from clean, sustainable, and renewable energy sources is necessary. Solar radiation is an unlimited form of clean and renewable energy. Its low cost and efficient harvesting can endlessly fuel our civilization. To date, the conventional silicon based solar cells have dominated the photovoltaic (PV) market because of its superior stability and high power conversion efficiency (PCE). Its highest efficiency surpassing 26% recorded at standard test conditions [1]. However, the initial production cost associated with silicon wafers used in this technology was very high. Finding alternative technologies to Si solar cells, which can compete in providing high PCE, excellent stability, high reproducibility and low cost, are still challenges for scientific community.

In a short span of less than 10 years, organo-metal halide perovskites (OMHPs) have emerged as a champion photovoltaic technology. Its solution processed fabrication, lower manufacturing cost and high PCE, made perovskite solar cell a promising future photovoltaic technology [2,3]. The OMHPs are group of materials with a formula of ABX_3, where A and B represent cations of different sizes and X represent an anion. For perovskite solar cell (PSC), the most commonly used small organic-inorganic cations (A), are methyl-ammonium $CH_3NH_3^+$ [4,5], formamidinium $NH_2CH_3NH_2^+$ [6,7], and cesium Cs [8,9]. Pb^{2+}, Ge^{2+} and Sn^{2+} all belonging to the group-IV(A) family, are widely reported as a divalent metal cation (B) [10,11]. Whereas F^-, Cl^-, Br^- and I^- are the most used monovalent halogen anions (X) in PSCs [12].

Known for their exceptional optoelectronic properties, perovskite materials were subject of investigation in the late 19th century for their potential applications in light emitting diodes (LEDs) and field effect transistors (FETs) [13,14]. In 2009, Miyasaka and coworkers for the first time employed these materials in solar cells [15]. By successfully using of $CH_3NH_3PbBr_3$ and $CH_3NH_3PbI_3$ as a sensitizer in Dye-sensitized solar cells (DSSCs), efficiencies of 3.13% and 3.81% were obtained respectively [15]. These efficiencies were further elevated to 6.54% in 2011, when Lee et al., sensitized 3.6 µm-thick TiO_2 films with quantum dots of $CH_3NH_3PbI_3$ employing quantum-dot sensitized solar cell (QDSSC) architecture [16]. However, the fabricated devices degraded within minutes because the corrosive redox electrolyte dissolved the QDs. This forced the researchers to focus on all solid state perovskite devices. The very first all solid state perovskite based solar cell was reported in 2012 [17], where the liquid electrolyte was replaced by organic hole transport material, spiro-OMeTAD. This significantly improved the stability of perovskite devices with elevating efficiency to exceed 9% [17]. From then on many notable groups and researchers around the globe joined the perovskite fever [18] by reporting different device architectures such as mesoscopic n-i-p [19], plannar n-i-p [20], inverted mesoscopic p-i-n [21] and inverted plannar p-i-n [22]. One major factor deciding the performance of the PSC was the quality of perovskite films. To achieve high quality perovskite films many different depositing techniques were reported such as one-step solution deposition [23], two-steps solution deposition [24], vapor assisted deposition [25], thermal vapor deposition [26], blade coating [27], ink jet printing [28], spray coating [29], slot die coating, screen printing and other emerging techniques [30]. To enhance the stability and overall PCE of the devices, many different approaches had been investigated, such as solvent engineering, process engineering, band gap engineering and contact engineering [31].

Within a decade the overall PCE of perovskite solar cell has dramatically improved from 3.81% in 2009 to 25.2% in 2019 [32]. Lead (Pb) was used as a divalent metal cation in almost all high-performance devices [33]. The toxicity of lead is an established fact, and risk of lead being inevitably accumulating in the food chain increases many folds with lead hallide making water soluble lead compounds overtime [34]. It is therefore necessary, and compelling to common sense that perovskite solar cells must go lead free. With a smaller ionic radius of 73 (pm), a lower electronegativity and more covalent nature than Pb^{2+}, Ge^{2+} was thoroughly investigated by Stoumpos et al., as a potential candidate for replacing lead in PSCs [35]. The germanium perovskites crystallize in trigonal crystal structure having a bandgap of 1.9 eV for $MAGeI_3$ [36]. Although the theoretical calculated efficiency for $CsGeI_3$ is 27.9% [37], practically the efficiency remained under 1% for all germanium based PSCs because of the poor film quality and instability of the Ge^{2+} ion towards oxidation to Ge^{4+} [11,35]. Gratzel and group replaced Pb with Cu only to achieve a meager efficiency of 0.017% [38]. High effective mass of holes, low absorption coefficients and the low intrinsic conductivity of the employed perovskite layer proved to be the main causes of poor performance.

Tin (Sn) has emerged as the most promising alternative to lead because of the same isoelectronic configuration of s^2p^2, and has considerably high mobilities [10^2–10^3 cm^2 (V^{-1} s^{-1})] when used in perovskites as compared to conventional lead based perovskites [10–10^2 cm^2 (V^{-1} s^{-1})] [39]. However, the facile formation of Sn vacancies along with stability of Sn in 2^+ oxidation state is in question. In the presence of oxygen Sn^{2+} is known to be oxidized to Sn^{4+} oxidation state [40]. The oxidized Sn^{4+} behave

as a p-type dopant, and with a concentration of even less than 0.1% it has drastic effects on PCE of the device [41].

Eyeing large scale modules and commercialization of Sn based PSCs, device stability and performance must be addressed simultaneously. This review will focus on important breakthroughs reported for Sn based perovskite from 2014 to 2020 for aforementioned parameters. Factors playing key role in device performance enhancement will be discussed. Role of different cations and their composition as reported since 2014 will be summarized. Furthermore possibilities and challenges for large scale application of Sn based PSCs are profoundly summarized.

2. Methylammonium Tin Halides ($CH_3NH_3SnX_3$, X = I, Br, Cl)

In 2014 Snaith and coworkers reported the very first methylammonium tin iodide ($CH_3NH_3SnI_3$) based completely lead free PSC [42]. An efficiency of 6.4% was recorded for the best performing device. The perovskite layer was deposited by spin coating a solution having equimolar quantities of CH_3NH_3I and SnI_2 prepared in degassed N-dimethylformamide (DMF). Having a small band gap of 1.23 eV, the open circuit voltage (V_{OC}) for the best performing device showed a remarkable value of 0.88 V, with estimated loss of only 0.35 eV. A mobility of 1.6 cm^2 V^{-1} s^{-1} with diffusion length of 30 nm was calculated for $CH_3NH_3SnI_3$ perovskite films. While a diffusion length of almost 1 μm was reported for the lead based counterparts of $MASnI_3$ [43]. It was observed that for Sn based perovskites the diffusion lengths can be increased up to 1 μm by suppressing background concentration of holes. All devices were fabricated in inert environment and properly encapsulated to minimize the exposure of perovskite layers to oxygen and humidity. While stability of Sn based perovskites remained an issue, high PCE (6.4%) paved the way for further research.

In the same year Stoumpos et al., reported an overall PCE of 5.73% for band gap engineered $MASnI_{3-x}Br_x$ based perovskite devices [44]. It was observed that the conduction band edge of $MAPbI_3$ is 0.23 eV higher than that of $MASnI_3$, which was why devices fabricated with the later has lower open circuit voltage compared to $MAPbI_3$. In order to increase the V_{OC} of Sn based perovskite devices, band gap was tuned by substituting bromide atoms for iodide atoms. These band gap tuned perovskites were synthesized in nitrogen glove box by mixing stoichiometric amounts of MAX and SnX_2 (X = Br, I), finely homogenized in a mortar. Followed by sealing in silica ampules under 1×10^{-4} mbar vacuum and heated to 200 °C.

The absorption onset of these hybrid halide perovskites can be tuned by proper substitution of bromide atoms, using $MASnI_3$ having smallest optical band gap of 1.3 eV, and $MASnBr_3$ with the largest optical band gap of 2.15 eV. An increase in V_{OC} was observed with increasing Br content. A V_{OC} of 0.68 V was recorded for $MASnI_3$ which increased up to 0.88 V for $MASnBr_3$ based device. However, the short circuit current density (J_{SC}) showed an opposite trend and decreased from 16.30 mA·cm^{-2} for $MASnI_3$ to 8.26 mA·cm^{-2} for $MASnBr_3$ [44]. The best PCE of 5.73% was recorded for device with $MASnIBr_2$, having a V_{OC} of 0.82 V, J_{SC} of 12.30 mA·cm^{-2} and Fill Factor (FF) of 0.57. A considerable high photovoltaic performance and atmospheric stability still remained a major concern for these devices. However, when sealed with surlyn films and stored in nitrogen glove box, the fabricated cells retained 80% of their initial photovoltaic performance in the first 12 h, which was very encouraging. By applying advanced sealing techniques the stability can further be significantly improved.

In an attempt to enhance the perovskite film quality and morphology, in 2015 Kanatzidis group reported a solvent mediated crystallization for $MASnI_3$ based PSCs [45]. By doing so, they achieved a highly uniform and pin hole free perovskite films, with a J_{SC} reaching to 21 mA·cm^{-2} and overall PCE of 3.15%. Two major factors governing photovoltaic performance of Sn based PCSs are self-doping and film quality. The Sn perovskites were prone to easily decomposed in isopropanol along a fast reaction rate between methylammonium iodide and SnI_2 films. This lead to an uncontrolled crystallization process of Sn perovskite films resulting in a poor film quality with presence of micron sized pinholes [45,46].

Sn^{2+} has greater Lewis Acidity than Pb^{2+} [47] resulting in a fast reaction dynamics between SnI_2 and MAI. When using DMF as a solvent, for the same concentrations $MASnI_3$ will crystallize more rapidly than $MAPbI_3$ while making perovskite films. This rapid crystallization gives rise to defects in perovskite films. To address this issue Kanatzidis and coworkers employed solvent engineering, where they used dimethyl sulfoxide (DMSO) because of its strongly coordinated nature, relatively high boiling point (189 °C) than DMF and a low saturated vapor pressure (0.42 Torr at 20 °C) [47]. Two different perovskite films were prepared by using DMF and DMSO as solvents. The films prepared with DMF crystallized rapidly during spin coating resulting in a dark brown color. However, uniform and light yellow films were obtained during spin coating when DMSO was used as a solvent, which were then annealed at 100 °C for 15 min to obtain a black perovskite film.

These results were further confirmed by comparing the XRD patterns of both films before and after thermal annealing as shown in Figure 1. Annealing has no effect on the prepared films by using DMF as a solvent, as all the peaks corresponding to tetragonal $MASnI_3$ phase in space group P4mm, were observed before and after annealing. This confirms the films were crystallized before annealing and showed no change afterwards. While in films made with DMSO a totally different reflection pattern was observed before annealing, which corresponded to neither the starting materials nor expected perovskite films. The DMSO was known to form $MAPbI_3$.DMSO complex when used for lead based perovskite films [48]. Hence it was assumed that this pattern correspond to a similar intermediate solvated phase. Careful investigations of XRD pattern of this solvated phase revealed the presence of SnI_2.3DMSO, acting as a cation instead of $CH_3NH_3^+$ cation. Figure 1c shows the Fourier transform infrared spectroscopy (FTIR) spectra of C−S and S−O stretching vibrations from the Sn^{2+}-coordinated DMSO solvent at 960 and 1012 cm^{-1}, respectively. After annealing this phase disappeared and was converted to $MASnI_3$. Compared to DMF, the DMSO as a solvent in perovskite films yielded much smoother, homogeneous and pin hole free perovskite films due to its controlled crystallization. Perovskite devices based on these films showed an overall PCE of 3.15%, with extraordinary J_{SC} of 21 $mA{\cdot}cm^{-2}$ and a moderate V_{OC} of 320 mV.

In a similar attempt, Bein and coworkers proved the usefulness of 1,4-dioxane mixed with methanol as a solvent for preparing high quality, pin hole free $MASnI_3$ perovskite films [49]. They choose a one-step spin coating route to prepare the perovskite films with precursors already dissolved in a mixture of MeOH:Dioxane. The perovskite was formed instantly after dropping the solution on spin coater because of the high vapor pressures of both MeOH and Dioxane. When compared with devices fabricated from DMF and DMSO as a solvent, device fabricated with MeOH:Dioxane mixture as a solvent yielded better photovoltaic results because of enhanced quality films and suppressed p-doping. An overall PCE of 1.05% was recorded for device fabricated with MeOH:Dioxane mixture which was considerably higher than that of devices fabricated with DMF and DMSO as solvents. While this method addressed issues of defects in thin films high background carrier density was still a major factor limiting PCE.

To reduce high background carrier density Kanatzidis and group proposed a process of reducing vapor atmosphere while preparing Sn based perovskite devices [50]. An overall PCE of 3.89% was achieved for $MASnI_3$ based devices employing this technique. Perovskite layer was prepared by spin coating a solution of $MASnI_3$ in the presence of hydrazine vapors. Hydrazine is a well-known reagent, which will reduce metal oxides and metal salts to pure metals. It is also used to reduce surrounding oxygen levels. The Sn perovskite films, when grown in the hydrazine atmosphere showed a reduction in Sn^{4+} impurities along with suppressing unfavorable reduction of Sn^{2+}.

By reducing Sn^{4+} to Sn^{2+}, Sn^{2+} vacancies are reduced, resulting in lowering p-type conductivity in perovskite films. Also the lower amount of Sn^{2+} vacancies resulted a decrease in anion antisite and cation antisite formation, further contributing to lowering of p-type self-doping [50]. Using this technique the Sn^{4+}/Sn^{2+} ratio was reduced by 45.8% compared to the ratios without using hydrazine atmosphere. This work was a significant step towards high performing $MASnI_3$ based devices, but stability remained a challenge.

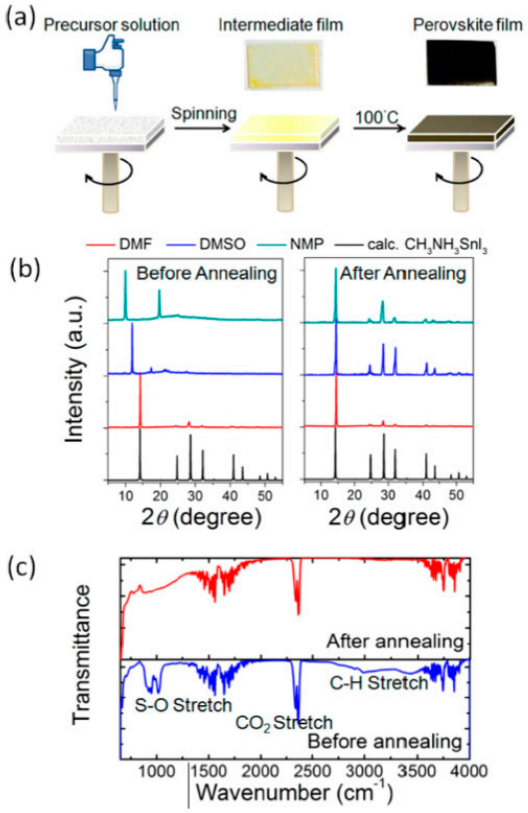

Figure 1. (**a**) Perovskite films prepared using DMSO as a solvent before and after annealing employing single step spin coating technique; (**b**) XRD patterns of the perovskite films using different solvents before (left) annealing and after (right) thermal treatment at 100 °C for 15 min; (**c**) FTIR spectra of the perovskite films deposited from a solution of DMSO before (Bottom) and after annealing (Top). At 960 cm^{-1} the characteristic C–S and at 1012 cm^{-1}, C–O stretching vibrations arising from Sn^{2+}- coordinated DMSO solvent can be seen before annealing. Adapted with permission from [45]. Copyright © 2015, American Chemical Society.

Kanatzidis and coworkers also suggested a low temperature vapor assisted solution process (LT-VASP) for minimizing p-type doping, reducing short circuiting and enhancing film quality for Sn based perovskites [51,52]. An overall PCE of 1.86% was reported for the best performing device. This method yielded better surface morphologies of perovskite films with great reproducibility and enhanced air stability. However, the first considerably stable $MASnI_3$ based perovskite films were reported by Horn et al. [53], where they used a two-step fabricating technique. These films showed remarkable stability as compared to all the earlier reported $MASnI_3$ films both in air and in nitrogen glove box. These stable perovskite films were obtained by depositing SnI_2 on FTO substrates using thermal evaporation of SnI_2 at a slow rate (2nm min^{-1}) in a vacuum. Followed by spin coating a solution of MAI in 2-propanol. Morphological studies as shown in Figure 2 revealed a higher coverage of substrate with perovskite crystals as compared to films synthesized using solution based processes.

Significant variations were observed in the sizes of perovskite crystals as the concentration of MAI solution changed. Few large crystals of 3–4 μm size were present, while rest of the substrate was covered by small 100–200 nm sized crystals when a 6 mg mL^{-1} solution of MAI was used. An increasing trend of crystal size was observed as concentration of MAI was increased however the crystal size again decreased for MAI solution with concentration of 40 mg mL^{-1} [53]. When exposed to air for an hour no visible change was observed in the color confirming the superior stability of these films with respect to films reported earlier. A 20 days old sample stored in nitrogen glove box showed no signs of degradation as no MAI or SnI_2 were present in it. Furthermore, when illuminated for

40 min along with exposure to air for 2 h these perovskite films retained 80% of their absorbance at 550 nm and no noticeable change in color was observed.

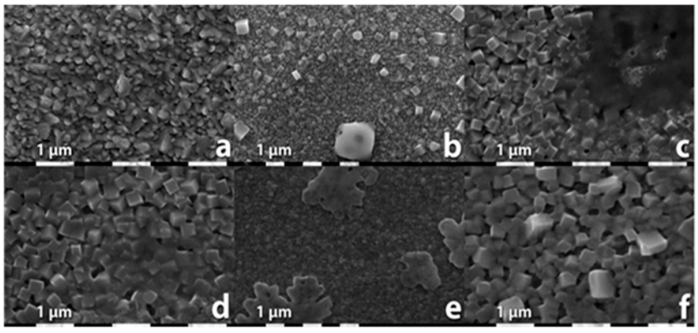

Figure 2. Images of different films as seen under SEM (**a**) Vapor-deposited 100 nm thick SnI_2 film; (**b**) $MASnI_3$ films prepared from a solution of 6 mg mL^{-1} using spin-coating technique (before annealing); (**c**) 10 mg mL^{-1}; (**d**) 20 mg mL^{-1}; (**e**) 40 mg mL^{-1} MAI solutions; (**f**) and a $MASnI_3$ perovskite film prepared using 20 mg mL^{-1} MAI followed by thermal treatment at 80 °C for 10 min. Adapted with permission from [53]. Copyright © 2015, WILEY-VCH Verlag GmbH & Co. KGaA, Weinheim.

The stability of $MASnI_3$ based devices was significantly increased by incorporating 5-ammonium valeric acid iodide (5-AVAI) in $MASnI_3$ films. Shigeeda et al., reported a very slow oxidation rate for $MASnI_3$ crystals when added with 5-AVAI [54]. When XRD patterns of films fabricated using just $MASnI_3$ and films fabricated using $MASnI_3$: 5-AVAI was compared. It was observed that for pure $MASnI_3$ films after 64.3 h half of the cubic phase has oxidized. Moreover most of the cubic phase is oxidized just after 88.5 h. However, in the case of 5-AVAI: $MASnI_3$ films (1:20) it took 113.5 h to oxidize half of the cubic phase, which was significant improvement in the device stability.

To further enhance the stability of $MASnI_3$ based perovskite devices, Adachi and group reported a unique method of combining anti-solvents with miscibilities, which are different than that of the precursor solvent [55]. Using this technique they significantly improved the coverage of the perovskite films. An overall PCE of 2.14 ± 0.35% was reported for planar perovskite solar cells prepared using these films. Morphology of perovskite film being a key player in deciding the overall performance of device, Adachi and coworkers controlled the crystallization of perovskite films using the SB method. In the SB method, anti-solvent bath was used to extract the good solvent in the precursor solution employing miscibility processes, where the miscibility between the solvents influences the extraction speed. By controlling the solvent extraction, growing of perovskite film is controlled. This method is also reported for Pb based perovskite solar cells and has been proved very effective in having smooth pin hole free perovskite films [56]. For $MASnI_3$ based perovskite devices the fabricated PSCs remained stable for over 200 h without degrading under standard 1 Sun illumination.

The stability of encapsulated devices based on $MASnI_3$ reached 500 h when Yamada et al., used SnF_2 incorporated $MASnI_3$ perovskite films [57]. Hao et al., previously used SnF_2 doping in $MASnI_3$ films to increase carrier diffusion length up to 500 nm [58]. Yamada and group reported a bandgap of 1.25 eV for SnF_2 doped $MASnI_3$ films, while films without SnF_2 doping showed an absorption edge that was significantly blue shifted. This blue shifted absorption edge in pure $MASnI_3$ films was assigned to unintentional p-type doping. SnF_2 addition increased the photocarrier lifetime by one order of magnitude. These encapsulated devices showed a PCE of 1.94% with an astonishing stability of 500 h under 1 Sun illumination [57].

The real breakthrough for stable methylammonium tin hallide based devices was reported in 2017 by Mohanta et al. [59] where they synthesized methyammonium mixed tri-halide tin ($MASnIBr_{2-x}Cl_x$) perovskites. Mohanta and group fabricated perovskite devices based on these films on a carbon based mesoscopic structure, making it free from both lead and hole transporting layer (HTM). Equimolar solution of MAI and $SnCl_2$/$SnBr_2$ were mixed in DMF. While keeping MAI at 100% the molar ratios

of $SnCl_2$/$SnBr_2$ were varied from 0/100, 10/90, 25/75, 50/50, 75/25 and 100/0 to vary I/Br/Cl ratios in perovskite films. The Eg = 1.81 eV along with spectral onset close to 700 nm was observed for films having 0% $SnCl_2$ ($MASnIBr_2$). A blue shift was observed as the ratio of $SnCl_2$ increased from 0 to 25%, confirming the presence of Cl within Sn perovskite films. A significant red shift was observed when $SnCl_2$/$SnBr_2$ ratio was increased to 50/50. Further increase in the ratios resulted in further red shift of absorption onset of perovskite films with the spectral edge touching 1000 nm for films made with 0% $SnBr_2$ and 100% $SnCl_2$ [59]. This technique resulted in having tin perovskite films with different proportions of halides such as $MASnIBr_2$, $MASnIBr_{1.5}Cl_{0.5}$ and $MASnIBr_{1.8}Cl_{0.2}$ producing PCE of 2.18%, 1.87% and 3.11% respectively. The best performance parameters were obtained for devices having $MASnIBr_{1.8}Cl_{0.2}$ as perovskite. A J_{SC} of 13.99 $mA{\cdot}cm^{-2}$ with a V_{OC} of 380 mV and a FF of 0.573 was recorded for this device. With a 3.11 % PCE the encapsulated device remained stable for over 2000 h which is quite remarkable.

The highest efficiency reported till date for $MASnI_3$ based PSCs is 7.78%, achieved through ion exchange/insertion reactions approach [60]. Song and group employed a very unique strategy of using SnF_2 and MAI as precursors for $MASnI_3$ perovskite films through ion exchange/insertion reactions. This unique method resulted in the formation of a very high quality perovskite film, having large amount of SnF_2 and very low concentration of Sn^{4+} [60]. The conversion steps are as follows:

$$SnF_2 + 2CH_3NH_3I \rightarrow SnI_2 + 2CH_3NH_3F \quad (1)$$

$$CH_3NH_3F \rightarrow CH_3NH_2\uparrow + HF\uparrow \quad (2)$$

$$SnI_2 + CH_3NH_3I \rightarrow CH_3NH_3SnI_3 \quad (3)$$

In the very first step of the perovskite film formation an ion exchange reaction took place between gaseous CH_3NH_3I and a solid state SnF_2, generating the intermediate SnI_2 and byproduct CH_3NH_3F. The byproduct is then removed via evaporation in the second step; while in the third step gaseous MAI reacted with SnI_2 to form the perovskite. It was observed that as the time of ion exchange/insertion reaction was increased from 5 min to 40 min the size of $MASnI_3$ crystals also increased forming a compact pinhole free perovskite film as shown in Figure 3. The perovskite films with excess SnF_2 obtained through this method were used in planner heterojunction structure (ITO/PEDOT:PSS/$MASnI_3$/$PC_{61}BM$/BCP/Ag) PSCs. Champion device produced an overall PCE of 7.78% with a stability of over 200 h for un-encapsulated devices tested under continuous 1 Sun illumination in N_2 atmosphere. Such a high efficiency with considerable stability is a very promising sign for the future of lead free perovskite devices. Table 1 summarizes the performance of best MA tin halide (s) based devices reported until 2020. Table 2 summarizes how the stability for MA tin based perovskite has shown increasing trend over the last few years.

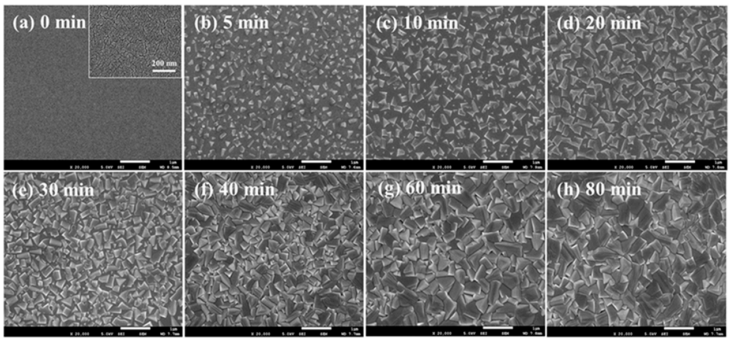

Figure 3. Surface SEM images of (**a**) pristine SnF_2/PEDOT:PSS film, and treated by the ion exchange/insertion reaction for; (**b**) 5 min; (**c**) 10 min; (**d**) 20 min; (**e**) 30 min; (**f**) 40 min; (**g**) 60 min; (**h**) 80 min. Adapted with permission from [60]. Copyright © 2020 The Authors. Published by WILEY-VCH Verlag GmbH & Co. KGaA, Weinheim.

Table 1. Performance of best MA tin halide (s) based devices reported until 2020.

Year	Device Architecture	Perovskite Film Fabrication Technique/PEROVSKITE Film	J_{SC} (mA·cm^{-2})	V_{OC} (V)	FF	EFF (%)	Ref.
2014	FTO/c-TiO_2/mp-TiO_2-Perovskite/HTL/Au	Spin Coating using DMF as solvent/$MASnI_3$	16.8	0.88	0.42	6.4	[42]
2014	FTO/c-TiO_2/mp-TiO_2-Perovskite/HTL/Au	Spin Coating using DMF as solvent/$MASnI_{3-x}Br_x$	12.3	0.82	0.57	5.73	[44]
2015	FTO/c-TiO_2/mp-TiO_2-Perovskite/Au	Spin Coating +Annealing using DMSO as solvent/$MASnI_3$	21.4	0.32	0.46	3.15	[45]
2016	FTO/c-TiO_2/mp-TiO_2-Perovskite/Au	LT-VASP/ $MASnI_3$	17.8	0.273	0.39	1.86	[51]
2016	ITO/PEDOT:PSS/Poly-TPD/$MASnI_3$/C_{60}/BCP/Ag	Thermal evaporation/$MASnI_3$	12.1	0.377	0.366	1.7	[61]
2017	ITO/PEDOT:PSS/$MASnI_3$/C_{60}/BCP/Ag	SB Method using DMSO as solvent/$MASnI_3$:SnF_2	11.82 ± 1.20	0.45 ± 0.01	0.40 ± 0.03	2.14 ± 0.35	[55]
2017	FTO/c-TiO_2/mp-TiO_2-perovskite/perovskite capping layer/PTAA/Au	Spin Coating in Hydrazine environment using DMSO as Solvent/$MASnI_3$	19.92	0.377	0.517	3.89	[50]
2017	FTO/c-TiO_2/mp-TiO_2-perovskite/ PTAA/Au	Spin Coating +Annealing using DMSO as solvent/$MASnI_3$:SnF_2	26.1	0.25	0.30	1.94	[57]
2017	FTO/c-TiO_2/mp-TiO_2-perovskite/Al_2O_3-Perovskite/C	Spin Coating using DMF as solvent/$MASnIBr_{2-x}Cl_x$	13.99	0.38	0.573	3.11	[59]
2020	ITO/PEDOT:PSS/$MASnI_3$/ $PC_{61}BM$/BCP/Ag	Ion exchange/insertion reactions/$MASnI_3$	20.68	0.57	0.66	7.78	[60]
2020	ITO/PEDOT:PSS/Perovskite/PCBM/PEI/Ag	Spin Coating in Nitrogen environment/$MASnI_3$	12.47	0.57	0.44	3.13	[62]

Table 2. Stability of MA tin halide(s) based perovskites.

Year	Device Architecture	Testing Environment	Stability	Ref.
2014	FTO/c-TiO_2/mp-TiO_2- $MASnI_{3-x}Br_x$ /HTL/Au	Devices were stored in nitrogen glove box and were sealed with Surlyn films	Retained almost 80% of initial performance for 12 h	[44]
2016	Two step process of vapor deposition + solution based technique to obtain $CH_3NH_3SnI_2$ films	Exposed to air and continuous illumination	Films retained almost 80% of their initial absorbance for 2 h	[53]
2016	5-AVAI:$MASnI_3$ films (1:20)	Exposed to air	113.5 h	[54]
2017	ITO/PEDOT:PSS/$MASnI_3$/ C_{60}/BCP/Ag	Under 1 Sun illumination	Devices retained 50% of their initial efficiencies for 200 h	[55]
2017	FTO/c-TiO_2/mp-TiO_2- $MASnI_3$:SnF_2/PTAA/Au	Encapsulated devices were kept under 1 Sun illumination in ambient conditions,	Devices were stable for 500 h	[57]
2017	FTO/c-TiO_2/mp-TiO_2-perovskite/Al_2O_3-$MASnIBr_{2-x}Cl_x$/C	Encapsulated devices while being stored	Retained 90% of their efficiencies for 2000 h	[59]
2020	ITO/PEDOT:PSS/$MASnI_3$/ $PC_{61}BM$/BCP/Ag	Un-encapsulated device under continuous 1 Sun illumination in inert environment	Retained almost 70% of initial performance for 200 h	[60]

Although, the MA based lead free perovskite devices produced some excellent efficiencies with considerable stability, the lack of control over p-doping has made it very difficult to have high level of reproducibility. Theoretical calculations performed on MA tin based perovskites confirmed that perovskite with MA are more likely to be oxidized than that of perovskites having $NH_2CH_3NH_2^+$ (FA) as cation [63]. The MA has smaller ionic sizes compared to FA, resulting in a strong antibonding coupling between Sn-s I-p, which consequently results in very high hole densities [64]. In order to have high efficiencies with excellent stability and reproducibility it is therefore necessary to explore other options instead of MA as a cation in lead free perovskite solar cells [62].

3. Formamidinium Tin Halides ($FASnX_3$, X = I, Br, Cl)

The $MAPbI_3$ was known to undergo a phase transition at 56 °C, changing its shape from tetragonal to cubic [65]. However, when MA was replaced by $NH_2CH_3NH_2^+$ (FA), the resulting perovskite $FAPbI_3$, does not show any phase transition until 150 °C. This enhancement of stability can be attributed to a comparatively rigid perovskite structure resulted from enhanced H bonding between organic cation and inorganic matrix [66]. Expecting the same for Sn perovskites, the very first work on formamidinium based tin perovskite was reported by Krishnamoorthy et al. [67] in 2015. An energy band gap of 1.41 eV, with a red shifted absorption onset (880 nm) compared to $FAPbI_3$ was observed for $FASnI_3$ perovskites. When left overnight, the color of pure $FASnI_3$ solution changed from yellow to orange. To solve this issue SnF_2 was added to the pure $FASnI_3$ solution in different molar ratios. Addition of SnF_2 not only increased the stability but also short circuit current of perovskite devices. The best $FASnI_3$ perovskite films were realized with films having 20 mol% SnF_2.

Perovskite devices fabricated with these films produced J_{sc} of 12.4 mA·cm^{-2}, V_{oc} of 262 mV, FF of 0.44 and overall PCE of 1.41%. To increase the J_{SC} of $FASnI_3$ based PSCs Koh and group increased the thickness of mesoporous TiO_2 from 350 nm to 500 nm [67]. This significantly reduced charge carrier recombinations inside the active material by providing more charge transfer sites. For the best performing device with 500 nm thick mesoporous TiO_2 layer, a short circuit current density of 24.45 mA·cm^{-2} was reported with a V_{OC} of 238 mV, fill factor of 0.36 and PCE of 2.10% respectively [67]. This pioneering work on $FASnI_3$ based perovskite provided a solid reason to explore and further optimize the performance of these devices for environment friendly and stable tin based PSCs. The real push towards a stable and highly efficient FA based tin halide perovskite came from Shin et al. [68] in 2016, when they fabricated a 100 day stable encapsulated perovskite device with a PCE of 4.8% using SnF_2-Pyrazine complex. To achieve this outstanding performance Shin and group deposited the perovskite film using both non solvent dripping process and solvent engineering technique [68].

They demonstrated that SnF_2 incorporated perovskite films made with only DMF as a solvent showed a very poor surface coverage and morphology (Figure 4a). The results were the same even for non-solvent dripping process (Figure 4b). But when solvent engineering was applied and films were grown from a mixture of DMF and DMSO in 4:1 volume respectively, a very smooth and uniform film was obtained (Figure 4c). However excess SnF_2 in the $FASnI_3$ films caused aggregation on top of film and few plate like aggregates were found on surface. These aggregates disappeared when pyrazine was also introduced along with DMF and DMSO in the solvent mixture (Figure 4d). This proved that pyrazine significantly improved the surface morphology by separation of phases induced by excess SnF_2. The surface of films prepared with SnF_2 addition oxidized 100% in air during fabrication process. However, Sn^{4+} content decreased in underneath layers. When pyrazine was added to films the oxidation decreased by 4-15% in each layer. When PSCs were fabricated using these optimized perovskite films a J_{SC} of 23.7 mA·cm^{-2}, V_{OC} of 320 mV, FF of 0.63 and PCE of 4.8% was recorded for the best performing device. These devices showed exceptional reproducibility and long term stability of 100 days in ambient conditions when encapsulated [68].

In addition to the same concept of solvent engineering and SnF_2 addition Zhao and group [69] modified perovskite formation by addition of diethyl ether dripping. This modification allowed them to achieve uniform provskite films with full surface coverage. The conventional n-i-p structure was also

replaced by p-i-n inverted architecture (ITO/PEDOT:PSS/$FASnI_3$/C_{60}/BCP/Ag) to avoid using salt-doped hole selective layers (HSLs), known to damage $FASnI_3$ perovskite [51,70]. Anti-solvent dripping is reported to enhance the quality of perovskite films [48] with toluene and chlorobenzene being the most popular choices. However, Zhao and group [69] observed that while using chlorobenzene or toluene to prepare $FASnI_3$ layers pin holes emerged in the surface of films because of rapid crystallization, reducing the quality of perovskites. When diethyl ether was used instead of chrolobenzene and toluene a comparatively slow crystallization rate was observed resulting in a pin hole free and smooth surface.

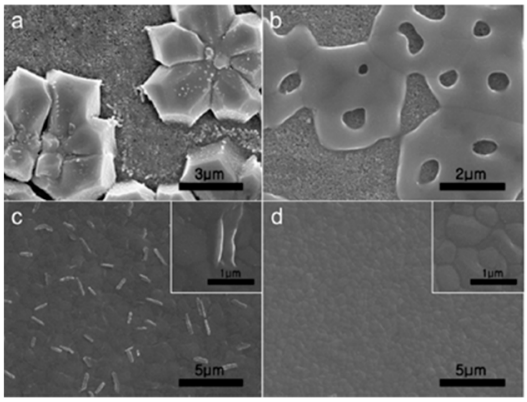

Figure 4. Images of $FASnI_3$ perovskite films produced using DMF as a solvent as seen under SEM; (**a**) without any nonsolvent dripping treatment; (**b**) with nonsolvent dripping. Images of $FASnI_3$ perovskite films produced using mixture of DMF and DMSO as solvent with nonsolvent dripping; (**c**) in the absence of pyrazine and (**d**) in the presence of pyrazine. Adapted with permission from [68]. Copyright © 2016, American Chemical Society.

A cross sectional view of inverted p-i-n PSC fabricated using these pin hole free, high quality $FASnI_3$ perovskites as seen under SEM is shown in Figure 5a. Where C_{60} and PEDOT:PSS acts as ESL and HSL respectively. The conduction band (CB) minima of $FASnI_3$ is well matched with the lowest unoccupied molecular orbital (LUMO) of C_{60} facilitating effective transfer of generated electrons from perovskite to Ag. The holes were blocked as the $FASnI_3$ has a valence band (VB) maxima above the highest occupied molecular orbital (HOMO) of C_{60} resulting in suppressing charge carrier recombination's at the interface. The best device provided a PCE of 6.22% with J_{SC} of 22.07 $mA{\cdot}cm^{-2}$, V_{OC} of 465 mV and FF of 60.67% under forward scan. A very small J-V hysteresis was observed due to invert device architecture. These fabricated devices showed good stability as a cell with PCE of 5.80% had only 5.86% decrease in performance even after 45 min. When kept in dark and inert environment devices were stable for 30 days. Zeng et al. [71] also used a similar approach with additional mixing of poly(α-methylstyrene) (PAMS) in diethyl ether dripping.

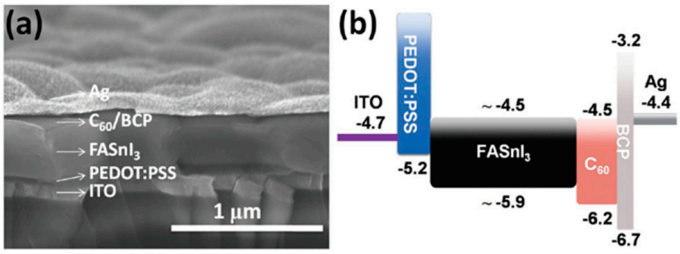

Figure 5. (**a**) A cross-sectional view of the fabricated device having 10 mol% SnF_2 additives as seen under SEM; (**b**) Energy level diagram. Adapted with permission from [69]. Copyright © 2016, WILEY-VCH Verlag GmbH & Co. KGaA, Weinheim.

In an attempt to improve the PCE of $FASnI_3$ based devices Kanatzidis and group suggested a thin layer of ZnS to be coated on top of mesoporous TiO_2 [72]. This cascade structure significantly reduced the interfacial recombination and enhanced the electron transfer capability. The best cell provided a PCE of 5.27% with V_{OC} of 380 mV, a short circuit current density of 23.09 $mA{\cdot}cm^{-2}$ and a FF of 60.01%. Kanatzidis and coworkers also fabricated a flexible $FASnI_3$ based perovskite with a PCE of 3.12% employing multichannel inter diffusion technique [73]. Perovskite films were prepared by spin coating mixture of FAI and PEDOT:PSS followed by annealing. SnI_2 film was then evaporated to have high quality, homogeneous $FASnI_3$ films. This fabrication technique allowed them to have a flexible PSC paving the way for commercializing of Sn based PSCs.

In the quest of achieving high PCE and considerable stability for lead free FA based tin PSCs Chueh et al. [74] used sequential deposition route. To form defect free homogeneous $FASnI_3$ films the reaction rate between FAI and SnI_2 was controlled. In the first step of deposition tri-methylamine (TMA) was incorporated in Sn solution to form SnY_2-TMA ($Y = I^-, F^-$) complexes [75] followed by intercalating with FAI to produce $FASnI_3$. This method allowed Jen and group to realize PCE of 4.34% and 7.09% for conventional n-i-p and inverted p-i-n PSCs, respectively [74]. When tested for stability the inverted device comparatively showed better stability than conventional device. In ambient air with 50% relative humidity the un-encapsulated devices degraded within the first 24 h. However, when stored in inert environment both devices retained more than 80% of their performance for 20 days. Figure 6 relates the PCE of devices with respect to storage time in different environments.

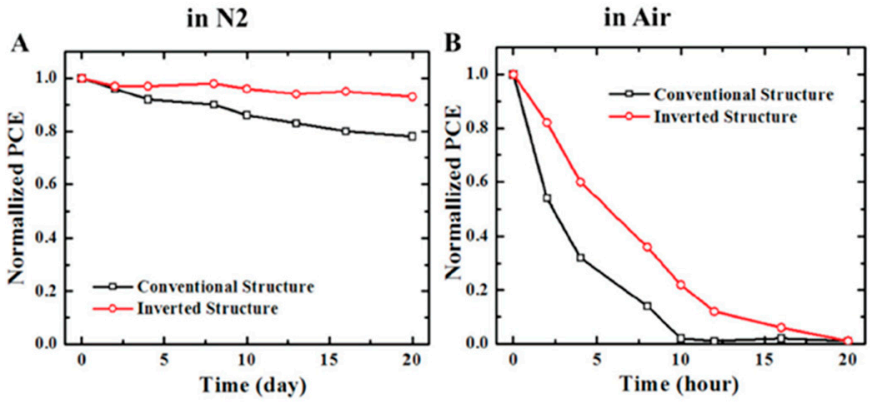

Figure 6. Room temperature stability tests of PSCs both in n-i-p and p-i-n architectures based on $FASnI_3$+SnF_2+TMA: (**A**) stored in N_2 environment and (**B**) stored in ambient condition (50% relative humidity). Adapted with permission from [74]. Copyright © 2017, WILEY-VCH Verlag GmbH & Co. KGaA, Weinheim.

As tin based perovskite is relatively new compared to Pb based perovskites, so many techniques that have already been proved useful for Pb based perovskties were applied to its Sn counterparts. It was well established with Pb perovskite lattice that introduction of Br atom in perovskite structure changed the shape from tetragonal to cubic. It also affected band gap and significantly improved the stability of these PSCs [76,77]. To enhance the stability of FASn halide based perovskite devices Lyu et al. [78] applied band gap engineering method to fabricate a considerably stable $FASnI_2Br$ perovskite with a band gap of 1.68 eV. When devices were fabricated from these perovskite films employing p-i-n architecture and with C_{60} as electron transport layer (ETL), a maximum PCE of 1.72% was recorded. When PCBM was used as ETL the efficiency dropped to 1.43% mainly because of a lower V_{OC}. However, the stability of un-encapsulated devices in nitrogen glove box increased from few hours to 30 h. This stability although is not enough, but the fact that it was recorded for un-encapsulated devices make it appealing. Applying proper encapsulation it can be significantly enhanced.

Using the same idea Shin et al. [79] incorporated Br atoms in $FASnI_3$ perovskite structure. The doping concentration of bromine was kept from 0 to 33 mol%. To investigate the effect of bromine

addition in crystal structure of $FASnI_3$ perovskites, films with and without bromine addition were prepared and their absorption spectra was measured for about 100 h while being exposed to air. The absorption of pure $FASnI_3$ films at 500 nm reduced to almost zero when exposed to air for 100 h while films with bromine maintained almost 40% of its initial absorption for the same time when tested under same conditions. This experiment further verified notion that addition of bromine not only shifts the band gap but also decrease Sn^{2+} oxidation, making films more stable in air.

The C-V measurements revealed that films produced with 25 mol% Br doped $FASnI_3$ have 3 order of magnitude less carrier density compared to film produced without any Br doping. This significant decrease of carrier density proved the initial assumption of Br doping reducing Sn^{2+} oxidation. A maximum PCE of 5.5% was obtained for Br doped device with a J_{SC} of 19.8 $mA{\cdot}cm^{-2}$, V_{OC} of 0.414 V and FF of 66.9%. When encapsulated these devices showed outstanding stability in ambient air, by retaining almost 100% of their initial performance for 600 h under continuous 1 Sun irradiation. Even after 1000 h only 17% reduction in the initial performance was observed for these remarkably stable Br doped $FASnI_3$ based PSCs. This considerably high efficiency along with remarkable stability was a great step towards lead free perovskite solar cells.

To further improve the PCE of $FASnI_3$ based devices Bian and group came up with a low cost solution of tin source purification [80]. Any commercial SnX_2 source contains Sn^{4+}, even those with 99% purity contain a significant concentration of oxidized Sn^{4+} resulting in poor performance and reproducibility issues. To solve this, Bian and coworkers added Sn powder to SnI_2. Tin powder reacts with Sn^{4+} and reduce it to Sn^{2+} state (Sn^{4+} + Sn >>>> $2Sn^{2+}$) [80]. A maximum PCE of 6.75% was achieved for inverted p-i-n architecture when annealing temperature and reaction time was optimized. However, the real breakthrough for record efficiency in $FASnI_3$ based devices was achieved in 2019 when Wu et al. [81] reported a 10.1% efficient device. To obtain a pin hole free film and control the grain boundaries Wu et al. [81] introduced π-conjugated Lewis base molecules during crystallization of $FASnI_3$ perovskite films.

The precursor solution for the films were prepared mixing 0.1%–1% in molar ratio, 2-cyano-3-[5-[4-(diphenylamino)phenyl]-2-thienyl]-propenoicacid (CDTA) in DMSO. During film fabrication this additive formed a stable intermediate phase and optimized the crystallization process of perovskite film by significantly slowing down the crystal formation. This method resulted in pin hole free and smooth $FASnI_3$ perovskite films with a larger carrier lifetime of 3.87 ns compared to pristine $FASnI_3$ film with a carrier lifetime of 2.09 ns. Perovskite devices were fabricated using these films employing ITO/PEDOT:PSS/$FASnI_3$/C_{60}/BCP/Ag architecture. The champion device with an active area of 0.09 cm^2 yielded record efficiency of 10.17% when 0.2% molar ratio of CDTA was used. The CDTA treatment of the perovskite films enhanced the V_{OC} to 0.63 V and FF to 74.7%. When tested for stability, the encapsulated device retained 90% of its initial performance even after 1000 h under continuous light soaking.

Recently Chen et al. [82] introduced [poly(ethylene-co-vinyl acetate) a unique polymer, as anti-solvent during spin coating $FASnI_3$ perovskite film. The C=O groups present in EVA had a very strong Lewis acid-base complexation with the uncoordinated tin atoms present in the perovskite film. This resulted in a considerably improved grain size, optimized orientation and significant decrease in surface defects of perovskite films. PSCs fabricated by this method gave a PCE of 7.72%, incorporating self-encapsulation properties. When tested for stability the un-encapsulated devices retained almost 62.4% of their initial efficiency even after 48 hr storage in ambient conditions with 60% relative humidity [82]. Such high efficiency along with self-encapsulation properties is a promising sign for future of highly efficient and stable lead free perovskite solar cells. Table 3 summarizes the performance of best FA tin halide (s) based devices reported until 2020 while, Table 4 includes the stability profiles of FA tin halide (s) reported until 2020.

Table 3. Performance of best FA tin halide (s) based devices reported until 2020.

Year	Device Architecture	Perovskite Film Fabrication Technique/Perovskite Film	J_{SC} ($mA \cdot cm^{-2}$)	V_{OC} (V)	FF	EFF (%)	Ref.
2015	FTO/c-TiO_2/mp-TiO_2-Perovskite/spiro-OMeTAD/Au	Spin Coating + Annealing/$FASnI_3$ +SnF_2	24.45	0.238	0.36	2.10	[67]
2016	ITO/PEDOT:PSS/Perovskite/C_{60}/Ca/Al	Spin Coating using DMF as solvent + chlorobenzene dripping + Annealing/$FASnI_2Br$	6.82	0.467	0.543	1.72	[78]
2016	FTO/c-TiO_2/mp-TiO_2-Perovskite/Spiro-OMeTAD/Au	Spin Coating using DMF+DMSO as solvent + Annealing/$FASnI_3$ + SnF_2 + Pyrazine	23.7	0.32	0.63	4.8	[68]
2016	ITO/PEDOT:PSS/Perovskite/C_{60}/BCP/Ag	Spin Coating using DMF+DMSO as solvent + diethyl ether dripping + Annealing/$FASnI_3$+SnF_2	22.07	0.465	0.606	6.22	[69]
2016	FTO/c-TiO_2/mp-TiO_2-ZnS-Perovskite/PTAA/Au	Spin Coating using DMF+DMSO as solvent + diethyl ether dripping + Annealing/$FASnI_3$+SnF_2	23.09	0.380	0.601	5.27	[72]
2017	ITO/PEDOT:PSS/PP-Perovskite/C_{60}/ BCP/Ag	Spin Coating FAI:PEDOT:PSS using water as solvent + Annealing + Evaporation of SnI_2/$FASnI_3$	17.78	0.33	0.679	3.98	[73]
2017	FTO/c-TiO_2/mp-TiO_2-Perovskite /spiro-OMeTAD/Au	Spin Coating using DMF+DMSO as solvent/$FASnI_{3-x}Br_x$ + SnF_2 + Pyrazine	19.8	0.414	0.669	5.5	[79]
2018	ITO/PEDOT:PSS/Perovskite/C_{60}:1 wt% TBAI/Ag	Sequential Deposition Route/$FASnI_3$ + SnF_2 + TMA	22.45	0.47	0.678	7.09	[74]
2018	ITO/PEDOT:PSS/Perovskite/ C_{60}/ BCP/Ag.	Adding Sn powder in precursor solution + Spin Coating using DMSO as solvent+ Annealing/$FASnI_3$+SnF_2	17.5	0.58	0.663	6.75	[80]
2019	ITO/PEDOT:PSS/Perovskite/ PCBM/BCP/Ag	Spin Coating using DMF+DMSO as solvent + diethyl ether blended with PAMS dripping + Annealing/$FASnI_3$	17.64	0.314	0.410	2.28	[71]
2019	ITO/PEDOT:PSS/Perovskite/C_{60} /BCP/Ag	Adding CDTA in precursor solution + Spin Coating using DMSO as solvent+ CB dripping + Annealing/ $FASnI_3$ + CDTA + SnF_2	21.22	0.63	0.747	10.17	[81]
2020	ITO/PEDOT:PSS/Perovskite/ PCBM/PEI/Ag	Spin Coating in Nitrogen environment/$FASnI_3$	15.36	0.64	0.56	5.51	[62]
2020	ITO/PEDOT:PSS/perovskite /PC_{61}BM/BCP/Ag	Spin Coating + EVA in CB as dripping/$FASnI_3$-EVA	22.80	0.523	0.646	7.72	[82]

Table 4. Stability of FA tin halide(s) based perovskites.

Year	Device Architecture	Testing Environment	Stability	Ref.
2016	ITO/PEDOT:PSS/ $FASnI_2Br$ /C_{60}/Ca/Al	Un-encapsulated devices were stored in nitrogen environment	Retained over 60% of their initial efficiency for more than 30 h	[78]
2016	ITO/PEDOT:PSS/$FASnI_3$ + SnF_2/C_{60}/BCP/Ag	Encapsulated devices stored in dark under inert environment	Retained almost 85% efficiency for 720 h	[69]
2016	FTO/c-TiO_2/mp-TiO2- $FASnI_3$ + SnF_2 + Pyrazine/Spiro-OMeTAD/Au	Encapsulated devices stored in dark under ambient conditions	Retained almost 98% of their initial efficiencies for 2400 h	[68]
2017	FTO/c-TiO_2/mp-TiO_2- $FASnI_{3-x}Br_x$ + SnF_2+ Pyrazine /spiro-OMeTAD/Au	Encapsulated devices under continuous 1 Sun irradiation in ambient environment	Retained almost 83% of initial performance after 1000 h	[79]
2018	ITO/PEDOT:PSS/$FASnI_3$ + SnF_2 + TMA/C_{60}:1 wt% TBAI/Ag	Encapsulated devices stored in ambient conditions	Retained almost 80% of initial performance for 420 h	[74]
2019	ITO/PEDOT:PSS/$FASnI_3$ + CDTA + SnF_2/C_{60}/BCP/Ag	Encapsulated devices under continuous 1 Sun irradiation	Retained almost 90% of its initial efficiency for 1000 h	[81]
2020	ITO/PEDOT:PSS/$FASnI_3$-EVA /PC_{61}BM/BCP/Ag	Un-encapsulated devices stored in ambient conditions with RH of 60%	Retained 62.4% of their initial efficiencies for 48 h	[82]

4. Cesium Tin Halides ($CsSnX_3$, X = I, Br, Cl)

Kanatzidis and coworkers were the very first to demonstrate effective use of $CsSnI_3$ in all solid state DSSC as a hole transport material [83]. The commonly used corrosive redox electrolyte was replaced with $CsSnI_3$ to realize efficiencies up to 10.2% in the DSSCs. The first use of $CsSnI_3$ as light harvesting material was reported by Wang et al. [84] in 2012, when a simple configuration of ITO/$CsSnI_3$/Au/Ti produced a PCE of 0.9%. To produce the perovskite film $SnCl_2$/CsI stack was deposited by e-beam deposition and thermal evaporation of CsI and $SnCl_2$, respectively. Followed by annealing at 175 °C for 1 min. This process created a single phased, dense and black colored polycrystalline perovskite film with a grain size of 300 nm. The Schottky solar cell based on these films provided a V_{OC} of 0.42 V, with a J_{SC} of 4.80 mA·cm^{-2}, FF of 22% and PCE of 0.9%.

Kumar et al., were also among the very first researchers who reported the use of $CsSnI_3$ in perovskite solar cells [85]. With a band gap close to ideal (1.3 eV) [83] and higher theoretical limit of achievable J_{SC} (34.3 mA·cm^{-2}) than its lead based counterparts (25.9 mA·cm^{-2}) [86], this material was expected to yield extraordinary efficiencies. However, theoretical calculations revealed that although the material is a semiconductor, it exhibit metallic characteristics with a very high hole mobility arising from intrinsic defects associated with Sn-cation vacancies [87]. To control this metallic conductivity Kumar et al., added SnF_2 to $CsSnI_3$. Perovskite films were prepared by Stichometric mixing of SnI_2, SnF_2 and CsI in proper solvents followed by spin coating and thermal annealing (70 °C). Perovskite solar cells employing conventional n-i-p architecture (FTO/c-TiO_2/mp-TiO_s-$CsSnI_3$+SnF_2/HTM/Au) were fabricated using 4′, 4– 4,-tris (N,N-phenyl-3-methylamino) triphenylamine (m-MTDATA) as hole transport material.

To compare performance and effect of SnF_2 on Sn vacancies, $CsSnI_3$ pervoskite films with 0, 5, 10, 20 and 40 mol% of SnF_2 were used. Devices without any SnF_2 doping were not functioning at all, while devices with SnF_2 doping were properly functioning with the best efficiency of 2.02% recorded for device with 20 mol% SnF_2 doping. These results were further explained by measuring the carrier densities of perovskite films. A very high carrier density of 10^{19} cm^{-3} was recorded for pure $CsSnI_3$ with holes as majority charge carriers. This p-type conductivity was caused by Sn-vacancies. With increasing mol % of SnF_2 the carrier densities tend to decrease. This proves that SnF_2 doping can significantly suppress Sn vacancies. Surprisingly, when stored in glove box these devices were stable for more than 250 h. While these devices show some stability, a very low open circuit voltage hinders the performance of these devices. With an astonishing J_{SC} of 22.70 mA·cm^{-2} obtained for the best performing device a very low V_{OC} of 0.24 V was recorded.

In an attempt to increase the V_{OC} of $CsSnI_3$ based perovskite devices the same group incorporated Br in $CsSnI_3$ perovskite structure [88]. As the bromine content was increased, the crystal structure of $CsSnI_3$ showed a phase transition from orthorhombic for $CsSnI_3$ to cubic for $CsSnIBr_2$ and $CsSnBr_3$ respectively. Also the optical bandgap of material changed from 1.27 eV for pure $CsSnI_3$ to 1.37 eV for $CsSnI_2Br$. For $CsSnIBr_2$ and $CsSnBr_3$ the optical bandgap of 1.65 eV and 1.75 eV was recorded respectively. The increasing bromine content also induced a change in the color of perovskite films from black to light brown, resulting in reduced light harvesting but simultaneously increasing the V_{OC}. Bromine doping also resulted for lowering charge carrier densities by one order of magnitude for $CsSnI_2Br$ (1.42×10^{17} cm^{-3}) and 2 order of magnitude for $CsSnIBr_2$ (6.32×10^{15} cm^{-3}) compared to pure $CsSnI_3$ films (5.28×10^{18} cm^{-3}) [88]. Overall the reduced charge carrier densities along with increase in the bandgap made it possible to achieve a maximum V_{OC} of 0.41 V for $CsSnBr_3$ based devices. However, this increase in the V_{OC} came at the expense of J_{SC}, and a very meager J_{SC} of 3.99 mA·cm^{-2} was recorded with a low PCE of 0.95%.

Remarkably Marshall and coworkers achieved a V_{OC} of 0.55 V using inverted p-i-n architecture (ITO|CuI|$CsSnI_3$|fullerene|BCP|Al) with indene-C_{60} bis-adduct (ICBA) as electron transport layer [89]. A 50 nm perovskite film prepared by spin coating 8 wt% $CsSnI_3$ in DMF was used as light harvester. To minimize charge carrier recombination's and enhance device stability the $CsSnI_3$ films were prepared using 10 mol% excess SnI_2. A highest efficiency of 2.76% was recorded for device incorporating these

perovskite films and using ICBA as ETL. The excess SnI_2 played a major role in deciding different performance parameters of fabricated devices. Firstly the excess SnI_2 provided a Sn rich source during perovskite formation which is known to suppress Sn vacancies and hence reduce background carrier density. Secondly it facilitated charge carriers transfer to CuI because of its favorable band alignment, reducing recombination losses. Most importantly the use of excess SnI_2 significantly improved device stability. When un-encapsulated devices fabricated without any excess SnI_2 lost almost 70% of their initial efficiency within 10 days while being stored in nitrogen glove box, surprisingly devices fabricated with 10 mol% excess SnI_2 retained 90% of their performance for the same period of time. The FF and V_{oc} of these devices remained stable even when exposed to air for 14 h.

The same approach was employed by Kanatzidi and coworkers to report one of the highest efficiencies of 4.81%, among all $CsSnX_3$ perovskite films based devices [90]. Perovskite films were produced from CsI/SnI_2 solutions in DMF and DMSO with different molar ratios starting from 0.1 reaching up to 1. As discussed in previous sections Kanatzidis and group used reducing vapor atmosphere as the films were produced in hydrazine environment to suppress Sn^{2+} oxidation during film formation. In conventional n-i-p architecture the best performance was recorded from devices incorporating films made with 0.4 molar ratio of CsI/SnI_2, having TiO_2 as ETL and PTAA doped with tetrakis(pentafluorophenyl)borate (TPFB) as HTL. When molar ratio was increased from 0.4, devices gave a low V_{OC} corresponding to high conductivities, while devices with molar ratio less than 0.4 gave poor J_{SC} due to lack of $CsSnI_3$ phase. A strong hydrazine environment was created in the glove box dropping 800µL on glass substrate while spinning it to have the PCE of 4.81% with J_{SC} of 25.71 $mA{\cdot}cm^{-2}$, V_{OC} of 381.66 mV and FF of 49.05%.

Marshall and group went on to investigate effectiveness of $SnCl_2$ addition, while preparing $CsSnI_3$ perovskites [91]. While devices prepared with 10 mol% of $SnCl_2$ presence during perovskite fabrication show no considerable effect on stability with respect to devices prepared with 10 mol% excess SnI_2, the efficiency jumped from 2.76% (as reported by the same group earlier) to 3.56%. Instead of incorporating Cl in the crystal lattice, the $SnCl_2$ formed a thin layer covering the perovskite crystallite surface. This resulted in a sacrificial oxidation of $SnCl_2$ layer when exposed to air, hence saving $CsSnI_3$ from oxidation. The elevated efficiencies using $SnCl_2$ can be attributed to lowering device performance parameters sensitivity to pin hole defects in the perovskite films. Because of its small size and lower mass the excess $SnCl_2$ present at the surface of the $CsSnI_3$ crystallites diffuse into fullerene layer causing its moderate n-doping. This resulted in forming a Schottky barrier limiting leakage current at ITO/Fullerene junction at the site of pinholes in the $CsSnI_3$ films.

Cahen and group reported an optimization strategy for $CsSnBr_3$ based devices by selecting different electron transport materials (ETM) and hole transport materials (HTM) layers for conventional n-i-p architecture based PSCs [92]. Devices were fabricated using TiO_2 and Al_2O_3 as ETM while PTAA, CBP and Spiro-MeOTAD were chosen as HTMs. By using TiO_2 as ETM, spiro-MeOTAD as HTM and 20 mol% SnF_2 doping, optimized PCE of 2.1% was achieved with a J_{SC} of 9.1 $mA{\cdot}cm^{-2}$, a V_{OC} of 0.42 V and a FF of 57%. All other combinations of HTM and ETM produced unsatisfactory results. The band alignment diagram of optimized device comparing effect of SnF_2 addition in $CsSnBr_3$ is given in Figure 7. When work function and ionization potential (valence band maximum, EVBM) of pristine $CsSnBr_3$ was compared to $CsSnBr_3$ doped with 20 mol% of SnF_2, the role of SnF_2 doping was revealed as it decreased work function (W_F) and the ionization potential of $CsSnBr_3$ as shown in Figure 7. This decrease in EVBM of $CsSnBr_3$ resulted in reducing the voltage loss by bringing it close to HOMO of spiro-MeOTAD.

Moghe and group fabricated $CsSnBr_3$ based PCSs using thermal deposition [93] to achieve 50 min stable devices under continuous 1 sun irradiation and ambient conditions without any encapsulation. Planar heterojunction architecture was selected for device fabrication with $CsSnBr_3$:SnF_2 sandwiched between MoO_3 and C_{60}. Figure 8a gives the band alignment diagram of fabricate devices. SnF_2 dopant was incorporated in the devices with different concentrations of 0%, 2.5%, 5% and 7.5%. The position of SnF_2 vapor deposited layer was also varied as shown in Figure 8. The best efficiency of 0.50% was

obtained for devices having 2.5 mol% of SnF_2 doping and SnF_2 layer sandwiched between CsBr and $SnBr_2$. While these devices are expected to have considerable stability when properly encapsulated, the low PCE limit its application on commercial scale. Kanatzidi's group further optimized the $CsSnBr_3$ perovskite layer by using hydrazine vapor atmosphere to grow $CsSnBr_3$ films [50]. This technique along its effects on perovskite layer has already been discussed in previous sections. Using reducing vapor atmosphere during $CsSnBr_3$ film growth they were able to suppress tin vacancies and reduce $Sn2^+$ oxidation. A maximum PCE of 3.04% was recorded for $CsSnBr_3$ based devices.

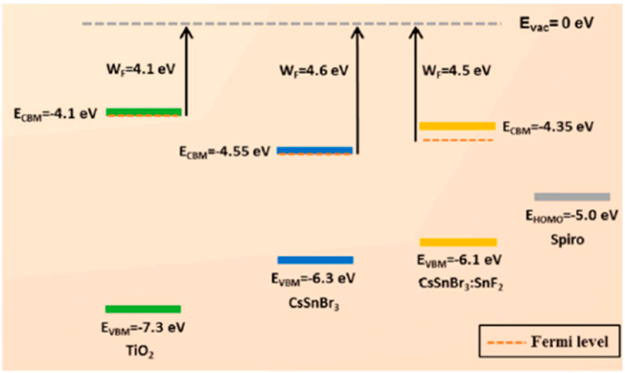

Figure 7. VBM energies from UPS measurements and CBM energies calculated using the UPS measurements and the optical band gap, i.e., neglecting the exciton binding energy, and the Fermi level (from UPS data) of dense TiO_2, pristine $CsSnBr_3$, and $CsSnBr_3$ (with 20 mol% SnF_2). Adapted with permission from [92]. Copyright © 2016, American Chemical Society.

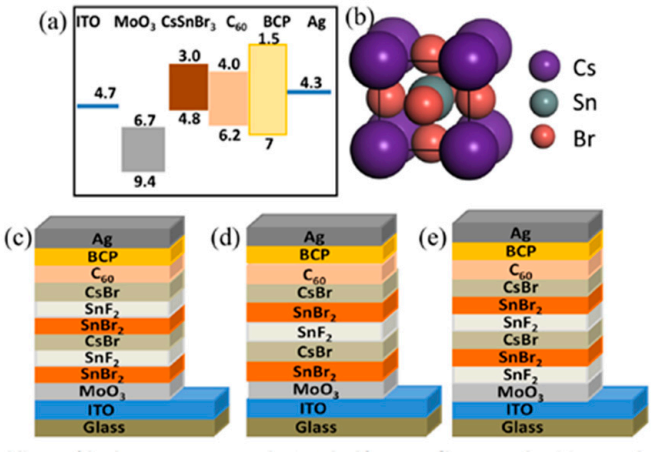

Figure 8. (**a**) Band alignment diagram of the planar $CsSnBr_3$ structure; (**b**) Crystal structure of $CsSnBr_3$; (**c**) SnF_2 layers splitting $SnBr_2$-CsBr layers in configuration 1(C1); (**d**) Single SnF_2 layer is inserted in configuration 2(C2), and (**e**) SnF_2 is inserted as split layer before $SnBr_2$ in configuration 3(C3). Adapted with permission from [93]. Copyright © 2016, Elsevier Limited.

In a similar attempt of enhancing the performance of $CsSnX_3$ based devices, Kanatzidi's group explored the possible effects of adding Piperazine to precursor solution of $CsSnI_3$ perovskite films [94]. Adding piperazine significantly suppressed the self-doping of the perovskite films and increased surface coverage while simultaneously reducing the crystallization of excess SnI_2. Perovskite films were spin coated keeping ratio of CsI/SnI_2 as 0.4. The molar ratio of piperazine to tin was changed from 0 to 25% by adding 2 M of piperazine solution to $CsSnI_3$ solution. Films were annealed at 90 °C for 25 min. Addition of piperazine significantly improved the film coverage by suppressing excess

SnI_2 crystallization. Figure 9 reveals the morphologies of perovskite films prepared from 0, 10 and 20 mol% of piperazine addition as seen under scanning electron microscope (SEM).

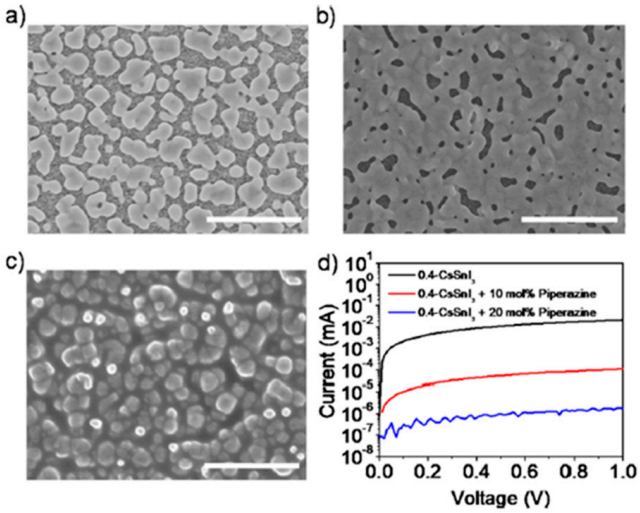

Figure 9. 0.4-$CsSnI_3$ perovskite films on top of meso-TiO_2 substrates as seen under SEM. When prepared with molar ratios of piperazine: (**a**) 0 mol%; (**b**) 10 mol%; and (**c**) 20 mol%. Scale bar represent length of 2 μm; (**d**) Semilog plot of the I-V characteristics for each condition. The measurements were performed using the four point probe technique. Adapted with permission from [94]. Copyright © 2018, American Chemical Society.

When no piperazine was added, the excess SnI_2 crystallized resulting in poor surface coverage. However, with piperazine addition the surface coverage enhanced as can be seen in Figure 9b,c. Addition of piperazine significantly increased the resistance of films as can be seen in Figure 9d. With 20 mol% of piperazine with resistance of perovskite films increased almost 4 orders of magnitude compared to resistance of pristine $CsSnI_3$ films. An optimized device was fabricated using 10 mol% of SnF_2 doping and 15 mol% of piperazine addition to achieve a maximum PCE of 3.83% with a J_{SC} of 20.63 mA·cm^{-2}, V_{OC} of 0.338 V and a FF of 54.18%. Although, the efficiency increased significantly the stability of these devices still remained considerably low.

In 2016 Li et al., reported 77 day stable $CsSnIBr_2$ films based devices [95]. This extraordinary stability was achieved by adding hypophosphorous acid (HPA) to precursor solution of $CsSnIBr_2$ perovskite films. Addition of HPA in precursor solution made tiny clusters of $CsSnX_3$–HPA_y (X = Br, I). These tiny clusters promoted growth of perovskite crystals by removing the redundant SnF_2, hence suppressing phase separation. When films were tested for conductivity, samples prepared with HPA had one order of magnitude less conductivity then those prepared without any HPA addition. Moreover, the charge carrier density reduced by one order of magnitude for films prepared with HPA addition (1.5×10^{15} cm^{-3}) compared to film prepared without any HPA addition (1.6×10^{16} cm^{-3}). Overall addition of HPA proved effective in reducing trap densities and Sn vacancies in $CsSnIBr_2$ films. The best device was fabricated with 0.5 μL mL^{-1} concentration of HPA acid, presenting efficiency of 3.02% with a J_{SC} of 17.4 mA·cm^{-2}, a V_{OC} of 0.31 V and Fill factor of 56%. When encapsulated these devices retained almost all of their initial performance for a time period of 77 days in ambient conditions. This extraordinary stability with moderate efficiency demonstrated the effective use of $CsSnIBr_2$ perovskite layer in lead free stable perovskite devices, paving the way for its commercial applications.

Sun and coworkers reported 3.31% efficient perovskite device based on a coarse grain B-γ-$CsSnI_3$ perovskite film [96]. A single step spin coating technique was employed to produce the perovskite films from the precursor solution, followed by 2 min annealing at 100 °C, 150 °C, 200 °C, 250 °C and 300 °C. The grain size showed an increasing trend with increase in annealing temperature as can be

observed in Figure 10. Grain size averaged 50 nm for films without any temperature treatment. For films annealed at 100 °C average grain size of 100 nm was reported, which further increased to 350 nm for 150 °C annealing temperature. Figure 10G represents the annealing temperature vs. average grain size.

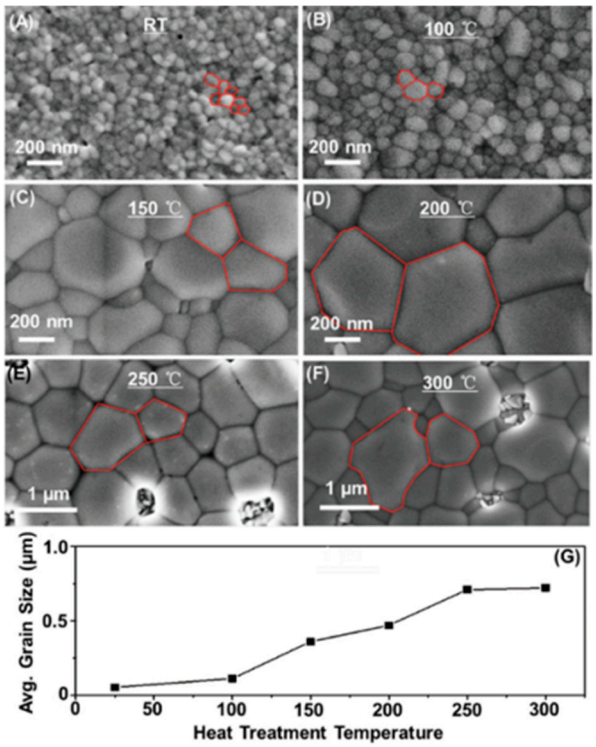

Figure 10. Top view of the B-γ-$CsSnI_3$ perovskite films as seen under SEM. (**A**) as-deposited; (**B**) annealed at 100 °C for 2 min; (**C**) annealed at 150 °C for 2 min; (**D**) annealed at 200 °C for 2 min; (**E**) annealed at 250 °C for 2 min and (**F**) annealed at 300 °C for 2 min; (**G**) Average grain size of the B-γ-$CsSnI_3$ thin films show increasing trend as the annealing temperature is increased. Adapted with permission from [96]. Copyright © 2016, WILEY-VCH Verlag GmbH & Co. KGaA, Weinheim.

It was confirmed from both theoretical and experimental calculations that as annealing temperature increased number of Sn vacancies also increased. Devices with different architectures were fabricated and tested for photovoltaic parameters. Devices having TiO_2 as ETL and Spiro-OMeTAD as HTL in conventional n-i-p architecture showed almost no performance when incorporated with B-γ-$CsSnI_3$ annealed at 100 °C as perovskite layer. When TiO_2 was replaced by Al_2O_3 as ETL in the same architecture, a very meager efficiency of 0.32% was achieved. A low crystallinity, perovskite making non ideal interfaces with scaffold material and presence of impurities, such as Y-$CsSnI_3$ and Cs_2SnI_6 were identified as causes of poor performance. To address these issues an inverted p-i-n architecture was used with a compact p-type nickel oxide (NiO_x) as HTL, PCBM as ETL and the perovskite layer was annealed at 150 °C. This device gave an outstanding efficiency of 3.31% with a J_{SC} of 10.21 mA·cm^{-2}, V_{OC} of 0.52 V and a FF of 62.5%.

During the past few years many unique attempts were also reported to elevate the efficiency and enhance the stability of inorganic Sn based perovskite solar cells. Chen and group reported $CsSnX_3$ based quantum rods to achieve a champion cell efficiency of 12.96% [97]. Quantum rods of $CsSnI_3$, $CsSnBr_3$ and $CsSnCl_3$ were synthesized respectively by solvothermal method as described in literature [97]. These high quality rods had lengths of several tens of nanometers with a diameter of 5 nm. The image of these rods as seen under transmission electron microscope (TEM) along with its elemental mapping from TEM energy-dispersive X-ray spectroscopy (EDS) is shown in Figure 11.

PSCs were fabricated in planar p-i-n heterojucntion architecture using these $CsSnX_3$ quantum rods as perovksite layers. The best PCE of 12.96% was obtained for devices based on $CsSnI_3$ quantum rods, whereas devices based on $CsSnBr_3$ and $CsSnCl_3$ quantum rods yielded efficiencies of 9.66% and 10.46% respectively. When tested for stability, devices fabricated with $CsSnI_3$ quantum rods remained stable for more than 240 h.

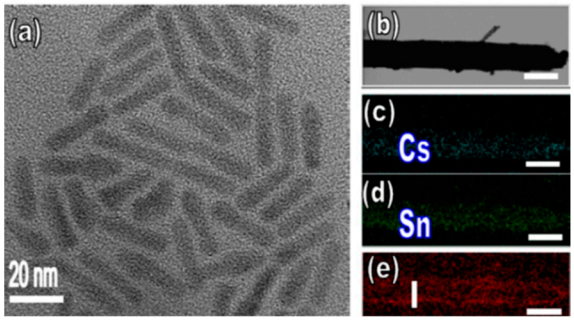

Figure 11. (**a**) $CsSnI_3$ Perovskite QRs as seen under TEM. (**b**–**e**) Selected zoom-in TEM images of several QRs: (**b**) A single $CsSnI_3$ perovskite QR as seen under TEM with corresponding energy dispersive spectroscopy (EDS) elemental mapping images, confirming that (**c**) Cs, (**d**) Sn, and (**e**) I are sequentially and uniformly spread over the entire surface of the $CsSnI_3$ QRs. The scale bars are 5 nm. Adapted with permission from [97]. Copyright © 2016, American Chemical Society.

Quan and coworkers reported 0D Cs_4SnX_6 nanocrystals having 21% Photoluminescence quantum yield (PLQY) [98] but with no considerable stability. In an attempt to enhance the air stability of perovskites Guo et al. [99] synthesized cubic nanocages of $CsSnBr_3$. When treated with perfluorooctanoic acid (PFOA), perovskite film of these $CsSnBr_3$ nanocages showed stability for over 24 h while being in ambient air. However in these unique approaches Kanatzidis and group were the first to report a considerably stable device based on Cs_2SnI_6 [100]. This material had a bandgap of 1.48 eV with a high absorption coefficient. While achieving a modest efficiency of 0.96% for the best device based on these perovskites, its stability remained outstanding. Un-encapsulated devices were stable for more than one week in ambient conditions which is quite remarkable. Recently Wang and group reported a 3% efficient $CsSnI_3$ based device by chemically doping cobaltocene ($CoCp_2$) into perovskite layer [101]. Doping of $CoCp_2$ into $CsSnI_3$ helped create a reducing environment which resulted in effective suppression of Sn^{2+} oxidation. This method also considerably enhanced the overall stability of these devices.

Although all the techniques discussed above for $CsSnI_3$ PSCs produced some excellent results, very recently Li et al. [102] reported one of state-of-the-art performance with a PCE of 3.8% and stability of 180 days. For the very first time vacuum flash-assisted solution processing (VASP) was used to fabricate the high quality $CsSnI_3$ perovskite films. The VASP method involved transferring the already spin coated Sn-based perovskite precursor to a vacuum (60 Pa) for 40 s. Followed by annealing at 60 C°for 10 min. The controlled solvent removal method allowed to produce high quality $CsSnI_3$ films with very few pin holes, reduced background charge carrier density and considerably enhanced perovskite stability. Films produced by VASP showed greatly improved stability than that of films produced using single step spin coating (controlled films). UV absorption spectrum revealed that at 450 nm VASP films retained 95% of their initial absorption even after 100 min exposure to air, while the controlled film retained only 85.5% absorption. The VASP PSCs yielded a PCE of 2% which increased to 3.8% upon storing in glove box for 3 months. The controlled PSC produced PCE of 1.1% and almost lost all of its performance within the first month of storage. As can be seen from Table 5 the performance of $CsSnX_3$ based devices has considerably progressed even in ambient conditions. These elevated efficiencies along with enhanced stability as given in Table 6 prove the importance of these devices in search of environment friendly highly efficient PSCs.

Table 5. Performance of best Cs tin halide (s) based devices reported until 2020.

Year	Device Architecture	Perovskite Film Fabrication Technique/Perovskite Film	J_{SC} ($mA \cdot cm^{-2}$)	V_{OC} (V)	FF	EFF (%)	Ref.
2014	FTO/c-TiO_2/mp-TiO_2-Perovskite/m-MTDATA/Au	Spin Coating using DMSO as solvent + Annealing/$CsSnI_3$ + SnF_2	22.70	0.24	0.37	2.02	[85]
2015	FTO/c-TiO_2/mp-TiO_2-Perovskite/Spiro-OMeTAD/Au	Spin Coating using DMSO as solvent + Annealing/$CsSnI_2Br$ + SnF_2	15.06	0.289	0.38	1.67	[88]
2015	ITO/CuI/Perovskite/ICBA/BCP/Al	Spin Coating using DMF as solvent + /$CsSnI_3$+excess SnI_2	12.30 ± 0.48	0.430 ± 0.061	0.395 ± 0.053	2.13 ± 0.53	[89]
2016	ITO/Perovskite/$PC_{61}BM$/BCP/Al	Spin Coating using DMF as solvent + Annealing/$CsSnI_3$+$SnCl_2$	9.89 ± 0.55	0.50 ± 0.01	0.68 ± 0.01	3.35 ± 0.21	[91]
2016	FTO/c-TiO_2/mp-TiO_2-Perovskite/Al_2O_3-Perovskite/ C-Perovskite	Spin Coating using DMSO as solvent + Annealing/$CsSnIBr_2$+SnF_2+ Hypophosphorous Acid (HPA)	16.7 ± 0.7	0.33± 0.02	0.53 ± 0.02	3 ± 0.2	[95]
2016	FTO/c-TiO_2/mp-TiO_2-Perovskite/Spiro-MeOTAD/Au	Spin Coating using DMSO as a Solvent + Annealing/$CsSnBr_3$+SnF_2	9.1	0.42	0.57	2.17	[92]
2016	ITO/MoO_3/Perovskite/C_{60}/BCP/Ag,	Vapor Deposition + Anealing/$CsSnBr_3$+ SnF_2 + Excess $SnBr_2$	2.1 ± 0.2	0.45 ± 0.05	0.52 ± 0.05	0.50 ± 0.05	[93]
2016	ITO/NiO_x/Perovskite/PCBM/Al	Spin Coating using a mixed polar Solvent + Annealing/B-γ-$CsSnI_3$	10.21	0.52	0.625	3.31	[96]
2016	ITO/mp-TiO_2-Quantum Rods of $CsSnI_3$/spiro-OMeTAD/Au	Spin Coating using $CsSnX_3$ perovskites (160 mg/mL) in toluene +Annealing/QRs of $CsSnI_3$	23.2	0.86	0.65	12.96	[97]
2017	FTO/c-TiO_2/mp-TiO_2-perovskite/perovskite capping layer /PTAA/Au	Spin Coating in Hydrazine environment using DMSO as Solvent/$CsSnBr_3$	13.96	0.366	0.593	3.04	[50]
2017	FTO/c-TiO_2/mp-TiO_2-Perovskite/PTAA/Au	Spin Coating using DMF + DMSO as solvent + Annealing + Hydraizne environment/ $CsSnI_3$+ Excess SnI_2	25.71	0.381	0.49	4.81	[90]
2017	FTO/c-TiO_2/Cs_2SnI_6/P3HT/Ag	Vapor deposition of CsI,SnI_2 + Solid State Reaction + Oxidation/Cs_2SnI_6	5.41	0.51	0.35,	0.96	[100]
2018	FTO/c-TiO_2/mp-TiO_2-Perovskite /PTAA/Au	Spin Coating using DMF+DMSO as solvent/$CsSnI_3$ + Excess SnI_2 + SnF_2 + Piperazine	20.63	0.338	0.541	3.83	[94]
2020	Mp-TiO_2/$CoCp_2$-$CsSnI_3$/Al_2O_3/NiO/ carbon framework	Drop Casting using DMSO as solvent + Annealing/$CoCp_2$-$CsSnI_3$	18.24	0.36	0.46	3	[101]
2020	ITO/Perovskite/C_{60}/BCP/Ag	Vacuum flash-assisted solution processing (VASP)/$CsSnI_3$	16.5	0.41	0.55	3.8	[102]

Table 6. Stability of Cs tin halide(s) based perovskites.

Year	Device Architecture	Testing Environment	Stability	Ref.
2014	FTO/c-TiO_2/mp-TiO_2- $CsSnI_3$ + SnF_2/m-MTDATA/Au	Devices stored in inert environment	Showed no significant loss of performance for almost 250 h	[85]
2015	ITO/CuI/$CsSnI_3$+excess SnI_2/ICBA/BCP/Al	Un-encapsulated devices tested under 1 Sun constant illumination in ambient conditions	Retained 70% of their initial efficiencies for 16 h	[89]
2016	ITO/MoO_3/ $CsSnBr_3$+ SnF_2+Excess $SnBr_2$/C_{60}/BCP/Ag,	Un-encapsulated devices tested under 1 Sun illumination in ambient conditions	Devices remained stable for 50 min	[93]
2016	ITO/mp-TiO_2-Quantum Rods of $CsSnI_3$/spiro-OMeTAD/Au	——	Sealed Devices remained stable for 240 h	[97]
2016	FTO/c-TiO_2/mp-TiO_2-Perovskite/Al_2O_3-$CsSnIBr_2$+SnF_2+ HPA/C-Perovskite	Encapsulated devices stored under ambient condition	Retained almost all of their initial efficiencies for 1848 h	[95]
2017	Cubic nanocages of $CsSnBr_3$	Ambient conditions	24 h stable	[99]
2020	ITO/VASP-$CsSnI_3$/C_{60}/BCP/Ag	Stored in inert environment	Increased its PCE from 2% to 3.8% after 2160 h	[102]

Over the years a steady progress has been made in elevating the efficiency and enhancing air stability of this single cation (MA, FA, Cs) based Sn perovskites. However, the challenge of commercialization has pushed the scientific and research community to come up with unique ideas. A new trend of combining two or more cations in a single perovskite has emerged, as it offers numerous possibilities of enhancing device performance and stability. This idea proved very successful in lead based perovskites [103–106], simultaneously gaining the attention of groups working on Sn based perovskites. The coming section summarize all work done in this regard based on Sn based perovskite, keeping in view the objective that high efficiency and long term stability should go hand to hand.

5. Mix-Cations (MC) Tin Halides ($MCSnX_3$, X = I, Br, Cl)

Liu and coworkers were the first to report a mixed cation $(FA)_x(MA)_{1-x}SnI_3$ perovskite in 2017 [107]. By employing an inverted p-i-n architecture for device fabrication and by optimizing the ratio of both cations within the perovskite layer, a maximum PCE of 8.12% was achieved. By changing the volume ratio x: (1–x) of $FASnI_3$ and $MASnI_3$ precursor solutions, different mixed cations perovskite layers were obtained with ratios of FA and MA as 0:100, 25:75, 50:50, 75:25 and 100:0 respectively. Perovskite films were realized by a one-step spin coating technique with chlorobenzene and SnF_2 addition to precursor solution made in DMSO. Bandgap of these films as calculated from photo luminescence (PL) spectra showed an increasing trend with the increase of FA content in films. For the films with FA:MA as 25:75 a bandgap of 1.28 eV was recorded, while for films with FA:MA as 50:50 and 75:25, bandgaps of 1.30 eV and 1.33 eV was recorded respectively. The morphological study of these mixed cation perovskite films revealed that films having lower FA content had few pin holes and low coverage, whereas films with higher FA content, $(FA)_{0.75}(MA)_{0.25}SnI_3$ and $FASnI_3$ was pin hole free and had complete coverage.

When devices were fabricated incorporating these mixed cations perovskite films a low average PCE of 3.61% ± 0.32% was obtained for $MASnI_3$ films. Moreover, with increasing FA content an increase in FF and V_{oc} was observed, with the best average PCE of 7.48% ± 0.52% recorded for devices based on $(FA)_{0.75}(MA)_{0.25}SnI_3$ perovskite films. The best device based on $(FA)_{0.75}(MA)_{0.25}SnI_3$ perovskite films gave maximum efficiency of 8.12% with a J_{SC} of 21.2 $mA{\cdot}cm^{-2}$, a V_{OC} of 0.61 V and a FF of 62.7%. This outstanding performance was attributed to the pin hole free and complete coverage of $(FA)_{0.75}(MA)_{0.25}SnI_3$ perovskite film. This combination of cations in perovskite significantly reduced the carrier recombination rate as was proved from transient state PL spectra and electrochemical impedance spectroscopy (EIS) of these films. $(FA)_{0.75}(MA)_{0.25}SnI_3$ had the highest PL lifetime of 3.07 ± 0.1 ns compared to other mixed cations perovskite films. At high applied voltages the value of R_{rec} recorded from EIS was also the largest for this combination among all perovskite films proving the effectiveness of reducing carrier recombination rate through cation mixing. These devices had a very high reproducibility with considerable stability. Under inert environment these PSCs retained 80% of their initial efficiency for more than 400 h.

To further improve coverage of $(FA)_{0.75}(MA)_{0.25}SnI_3$ perovskite films and increase the crystallite size Ozaki et al. [108] reported a hot antisolvent treatment (HAT) along with annealing in DMSO vapors. Pin hole free films with complete coverage were obtained when antisolvent was preheated to 65 °C before dripping (in this case chlorobenzene). A large density of perovskite nucleation sites were formed in the case of preheated antisolvent dripping technique, resulting in a pin hole free full coverage films. Whereas, films without HAT resulted in poor coverage, and had pin holes after annealing. When films were annealed in a mild DMSO vapor-enriched environment the quality of perovskite further increased and average crystallite size increased from 237 nm to 440 nm. Combining both of these optimizing strategies Ozaki et al. [108] were able to achieve a best PCE of 7.2%.

By employing solvent engineering technique, Yan et al. [109] were able to achieve efficiency of 9.06%. Different anti solvents such as toluene (TL), chlorobenzene (CB) and diethyl ether (DE) were used for perovskite film production. For optimum performance, SnF_2 was added to suppress Sn^{2+} oxidation and mixture of DMF as well as DMSO was used as a solvent in the perovskite precursors. When films were prepared without anti-solvent dripping it affected both, their crystallinity and crystal

orientation. The preferred orientation for perovskites without anti-solvent dripping was (120), while those prepared with anti-solvent dripping preferred (100) and (200) [109]. A morphological study of $(FA)_{0.75}(MA)_{0.25}SnI_3$ perovskite films prepared with and without anti-solvent dripping revealed that films produced without any anti-solvent treatment resulted in discontinuous films with several flower shaped grains as shown in Figure 12. This discontinuous film is resulted due to low number of nucleation sites. When anti-solvent treatment was applied number of nucleation sites considerably increased and a much smoother full coverage film was formed. As can be seen from Figure 12 with DE as anti-solvent higher number of pin holes are present, the number of pin holes dropped when TL was used. However, the best film having least number of pin holes was produced when CB was used as anti-solvent.

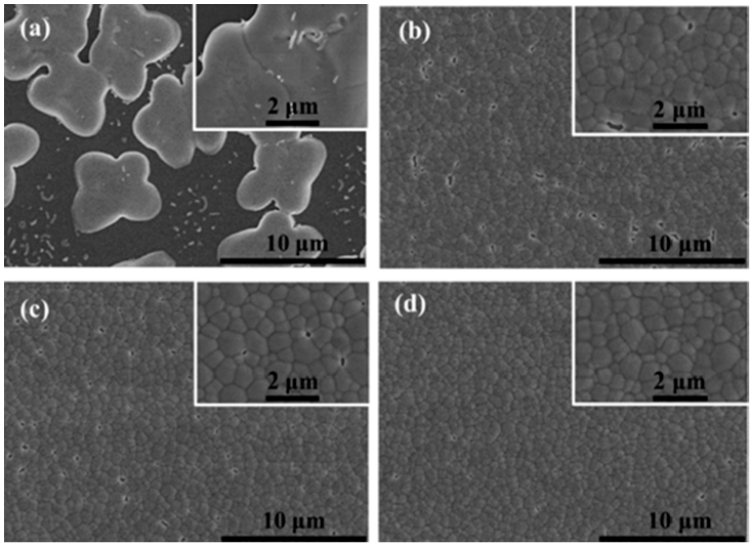

Figure 12. Top-view $(FA)_{0.75}(MA)_{0.25}SnI_3$ films deposited on ITO/PEDOT:PSS substrates as seen under SEM (**a**) without anti-solvent; (**b**) with DE; (**c**) with TL; and (**d**) with CB. Adapted with permission from [109]. Copyright © 2018, American Chemical Society.

Perovskite devices employing p-i-n architecture were fabricated based on these films using PEDOT:PSS as HTL and C_{60} as ETL. Films dripped by CB yielded the best PCE of 9.06%. Whereas films dripped with TL and DE gave PCE of 7.52% and 6.29% respectively. The high efficiency obtained from films dripped with CB was attributed to low charge carrier recombination rate resulted from pin hole free films with full coverage. At high applied voltages value of R_{rec} recorded from EIS was also the largest for CB dripped films based devices proving the effectiveness of reducing carrier recombination rate through CB dripping. When tested for stability, CB dripped perovskite films based encapsulated devices retained almost 75% of their initial efficiency over a period of 30 days when stored in nitrogen glove box.

Kanatzidi and group applied a different approach to enhance overall performance and improve air stability of lead free Sn based perovskite solar cells. Perovskite devices based on hollow ethylenediammonium $FASnI_3$ ({en}$FASnI_3$) were fabricated to achieve a PCE of 7.14% with enhanced air stability of more than 1000 h with proper encapsulation [110]. The incorporation of en in perovskite resulted in a novel 3D mixed cation perovskite ({en}$FASnI_3$), opening the door for tuning the bandgap without using solid solutions. This 3D hollow ({en}$FASnI_3$) was prepared by mixing stichometric amount of en and FAI in a solution of SnI_2, followed by adding it to a mix solvent of hydroiodic acid (HI) and H_3PO_2. Initially en/FA ratio was kept at 0%, 10% and 25% to determine the optimum amount of en loading. The crystal structure of {en}$FASnI_3$ retained the pseudocubic shape of pristine $FASnI_3$ and orthorhombic unit cell with very minor change in the unit cell volume. It was assumed that to

incorporate large sized en in 3D crystal structure other species, neutral or charged with proportionate size must be removed from crystal resulting in Schottky defects or point defects respectively.

To investigate the exact structure of this new mixed cation perovskite Kanatzidi and coworkers used many experimental techniques and theoretical calculations, all of which confirmed a hollow 3D structure with missing SnI_2 neutral fragments. This resulted in narrowing of both, VB and CB hence increasing the bandgap of these {en}$FASnI_3$ perovskites. Removal of SnI_2 units from the crystal structure, the observed decrease in energy levels of VB maxima automatically enhanced the stability of devices based on these perovskites as it shifted the absolute work function to lower energies resulting in reduction of oxidation tendency. A bandgap of 1.4, 1.5 and 1.9 eV was reported for perovskite materials with 0, 10 and 25% of en loading, respectively. Films with 0% en loading showed a carrier lifetime of 0.19 ns whereas a carrier lifetime of 0.46 and 0.68 ns was calculated for 10 and 25% en loading respectively. Perovskite devices employing n-i-p architecture were fabricated using these {en}$FASnI_3$ perovskties. Device based on pristine $FASnI_3$ yielded a PCE of 1.40%, whereas devices based on 10 and 25% of en loading gave PCE of 6.94% and 2.34%, respectively.

The relatively poor performance of pristine $FASnI_3$ based device was attributed to poor coverage and a very high carrier recombination rate. While low efficiency of 2.34% in devices based on 25% en loading was caused by a very low J_{sc} resulted from a high bandgap of 1.9 eV. These results proved the optimum value for en loading to be 10% where the champion cell achieved a PCE of 7.14% with a J_{SC} of 22.54 $mA{\cdot}cm^{-2}$, a V_{OC} of 0.480 V and a FF of 65.96% when measured under reverse voltage scan. When tested for stability the encapsulated devices retained 96% of their initial performance even after 1000 h which is a very encouraging prospect for the future of highly efficient and stable lead free tin based PSCs. Later Kanatzidis and group extended the same approach to fabricate highly efficient and stable {en}$MASnI_3$ and {en}$CsSnI_3$ perovskites [111]. The champion cell achieved a PCE of 6.63% for {en}$MASnI_3$ with 15% of en loading, while the best performance for {en}$CsSnI_3$ based solar cell was recorded for 10% of en loading with a PCE of 3.79%. This optimum en loading also significantly increased the air stability of both perovskites and PSCs based on them. Very recently Kanatzidis and group demonstrated the effective use of benzodithiophene (BDT)-based small organic molecules as hole transport materials for efficient lead free Sn based PSCs [112]. Efficiency of 7.59% was achieved for the champion device using these HTMs.

It was observed in the case of lead based perovskite devices that as the dimensionality of perovskite decreased the stability of device increased [113,114]. Keeping this in mind Kanatzidis and group reported 2D $(BA)_2(MA)_{n-1}Sn_nI_{3n+1}$ perovskites with enhanced moisture stability [115]. The optical band gaps of these 2D perovskites can be tuned from 1.83 eV (n = 1) to 1.20 eV (n = ∞), however for solar applications n = 3 and n = 4 were selected to have an optimal band gap of 1.50 and 1.42 eV respectively. To improve perovskite film morphology triethylphosphine (TEP) and SnF_2 was added to the precursor solution. Devices were fabricated using these perovskite films to test their performance and moisture stability. For value of n = 3 a maximum PCE of 1.94% was obtained, while devices with n = 4 yielded a PCE of 2.53 %. When compared for stability with $MASnI_3$ based devices, the encapsulated devices with n = 4 retained almost 90% of their initial efficiency for more than one month while in the same period the encapsulated devices based on $MASnI_3$ completely degraded. This enhanced stability of 2D $(BA)_2(MA)_{n-1}Sn_nI_{3n+1}$ perovskites based solar cell is attributed to the formation of long chains of hydrophobic butyl ammonium in the perovskite resulting in protecting perovskite films.

In 2017 Liao et al. [116] reported a 5.94% efficient and 100 h stable 2D $(PEA)_2(FA)_{n-1}Sn_nI_{3n+1}$ based perovskite solar cell. Very recently Liu et al. [117] demonstrated that different alkyl chain lengths have significant effects on crystal orientation and phase distribution in 2D perovskite films. Organic cations with short lengths of alkyl chains can increase dimensionality and can produce highly oriented crystal grains [117]. 2D/3D mixed cations ($PEA_xFA_{(1-x)}SnI_3$) Sn based PSC with a PCE of 6.98% was reported in 2018 by Xi et al. [118]. Incorporation of large PEA in perovskite structure significantly improved the PCE and stability of the 2D/3D mixed fabricated devices. A two-step fabrication route was used to

prepare (PEA,FA)SnI_3 bulk heterojunction perovskites. First PEAI molecules were evaporated to form PEAI/FAI mixture on top of FAI films followed by evaporation of SnI_2 forming a 2D/3D perovskite. To find the best combination different amounts of PEAI was evaporated such as 25, 50 and 75 mg. Devices were fabricated employing p-i-n planar heterojunction architecture with an ultrathin layer of LiF (3, 5 and 8 nm thick) deposited at ITO/PEDOT:PSS interface. This insulating LiF improved the hole extraction at ITO/PEDOT:PSS interface along with lowering the work function of PEDOT:PSS. The best performance was realized with 50 mg of PEAI evaporation along with keeping LiF thickness at 5 nm. The champion device provided a PCE of 6.98% with a J_{SC} of 20.07 mA·cm^{-2}, a V_{OC} of 0.47 V and a FF of 0.74. Shao et al. [119] reported a 9% efficient 2D/3D mixed highly crystalline $FASnI_3$ based perovskite solar cells. The perovskite films were prepared by mixing 0.08 M of 2D layered tin perovskite with 0.92 M of 3D $FASnI_3$ along 2-phenylethylammoniumiodide (PEAI).

Marshall and group reported a 3D mixed cation $Cs_{1-x}Rb_xSnI_3$ perovskite material for solar cell applications. By increasing the value of x open circuit voltage can be significantly increased in this type of perovskite material. However they observed that as the number of Rb atoms substituting Cs increased the stability of the perovskite decreased. The champion cell provided a PCE of 2.25% with 50% of Cs substituted by Rb and having 10 mol% of excess SnI_2 [120]. Ran et al. [121] reported a 2000 h stable perovskite device when stored in nitrogen filled glove box with a PCE of 6.08% by successfully doping Cs in $FASnI_3$ perovskite. Incorporating Cs into $FASnI_3$ improved the geometric symmetry of the crystal by inducing contraction of corner sharing SnI_6 octahedra. It also significantly enhanced the stability of perovskite by reducing Sn^{2+} oxidation tendency. Compared to pristine $FASnI_3$, absorption edge in UV-Vis spectra and PL spectra of $Cs_xFA_{1-x}SnI_3$ films were considerably red shifted. This red shift is attributed to reduction of band gap resulted from the contraction of crystal lattice due to incorporation of Cs. Details of optimization can be read from the published report [121], where the best PCE of 6.08% is reported for device based on perovskite film having 8% of CsI doping. This enhanced efficiency is attributed to reduction of hole trap density, increase of carrier motilities and reduction in bulk resistance for $Cs_xFA_{1-x}SnI_3$ films compared to pristine $FASnI_3$ films. The 8% doped CSI device showed an outstanding stability of 2000 h in nitrogen filled glove box by maintaining 90% of its initial performance in that time period. Compared with pristine $MASnI_3$ and $FASnI_3$ based devices Cs doped device had considerably improved stability both in nitrogen and in air.

Jokar et al. [122] reported addition of butylammonium iodide (BAI) and ethylenediammonium diiodide ($EDAI_2$) as additives in $FASnI_3$ based perovskite to achieve power efficiencies of 5.5% and 7.4% respectively. Addition of BAI in the $FASnI_3$ perovskite provided the benefit of lowering dimensionality of perovskite from 3D to a hybrid 2D/3D structure. Although this hybrid structure possessed advantages such as superior crystallinity and preferred crystallographic orientation, the surface was not pin hole free as was resulted from the slow nucleation and too rapid crystal growth rate. When BAI was replaced by di-ammonium cations a dense pin hole free perovskite film was produced as a result of the presence of two ammonium groups which increased interactions with Sn perovskite and ultimately controlling the crystal growth rate. These mixed cations perovskites were less likely to oxidize as compared to pristine $FASnI_3$ perovskites. Since, forming a compact layer and preventing water molecules to diffuse in the perovskite BAI successfully retarded the oxidation while in case of $EDAI_2$ the enhanced stability is attributed to it being a good reducing agent. Almost 90% of the initial efficiency was maintained by the encapsulated devices based on $FASnI_3$-BAI 15% for over 2000 h under inert environment. For devices based on $FASnI_3$-$EDAI_2$ 1% the efficiency gradually increased from its initial value of 6.3% to its maximum value of 8.9% after storing in nitrogen for 1462 h. This increase in performance is attributed to $EDAI_2$ slowly passivating the surface and gradually adjusting the crystal structure to its optimal phase near 1500 h [122]. Recently Weber et al. [123] reported a 4.63% efficient mixed cation perovskite device by mixing three different cations along with introducing bromide in the perovskite lattice. $MA_{0.75}FA_{0.15}PEA_{0.1}Sn(Br_xI_{1-x})_3$ was used as perovskite layer having an optical bandgap of 1.29 eV.

It was in 2019 when Jokar et al. [124] reported one of the most efficient and highly stable Sn based perovskite solar cell with a PCE of 8.5% recorded for fresh device. This extraordinary efficiency was achieved by incorporating a non-polar organic cation guanidinium ($CH_6N_3^+$, GA) in the perovskite crystal of $FASnI_3$ while simultaneously adding ethylenediammonium diiodide ($EDAI_2$) and SnF_2 to perovskite. Besides being a non-polar, Guanidinium has a size slightly larger (278 pm) than that of FA^+ (253 pm) [125]. When used in Sn based perovskite the $GASnI_3$ is reported to adopt a hexagonal shape with a bandgap of 1.9 and 2.1 eV for its 3D hexagonal and its 2D monoclinic structures respectively [126]. Perovskite films were prepared from precursor solutions of GAI and FAI with varying ratios and mixing them with equimolar SnI_2 solution. For enhancing performance and stability of perovskites, SnF_2 and $EDAI_2$ were also added in the mixture to obtain the final perovskite films of $GA_xFA_{1-x-2y}SnI_{3-y}EDAI_2$. As reported earlier by the same group incorporating trace amounts of $EADI_2$ in $FASnI_3$ perovskite produced pin hole free, uniform and dense perovskite films simultaneously reducing tendency of Sn^{2+} oxidation hence increasing stability [122]. As the ratio of GAI:FAI increased the size of perovskite crystal also increased resulted from the larger size of the GA. Incorporation of GA into the perovskite crystal also caused expansion of unit cell hence, increasing the lattice parameters. Increasing GAI proportion from 0 to 30, the absorption band edges of E1Gx perovskites correspondingly shifted towards smaller wavelengths. Whereas, bandgap energies increased from 1.44 eV for x = 0 to 1.53 eV for x = 30.

The optimal performance was recorded for device based on 20% GAI and 1% $EDAI_2$, represented as E1G20 this device yielded a champion PCE of 8.5% (8.3% certified). The efficiency continuously increased and reached 9.6% after 2000 h storage in nitrogen filled glove box. To test the champion device for stability, performance of device under three different test conditions were analyzed. For comparison device based on pristine $FASnI_3$ and device based on perovskite having only $EADI_2$ mixed in $FASnI_3$ (E1) was also tested under same conditions. As can be seen from Figure 13a the encapsulated E1G20 device remained stable for more than one h with negligible loss of PCE in air (RH = 50%) under continuous 1 Sun AM1.5G illumination. While under the same conditions encapsulated E1 device only sustained its maximum performance for 300 s and deteriorated quickly afterwards. When unencapsulated devices were stored in air (RH = 60%) devices based on pristine $FASnI_3$ lost their performance within two h, whereas E1G20 devices retained 80% of their initial performance for 96 h. The performance of E1G20 device was completely loss free for 170 h when was stored in air under 20% relative humidity as shown in Figure 13b. The same device when stored in nitrogen glove box for over 2000 h its PCE gradually increased with time from 7.3% to a maximum of 9.6%. Figure 13d represent the certified efficiency for E1G20 device.

Fu et al. [127] used a similar strategy of adding NH_2GACl to the perovskite film to passivate defects and decrease Sn^{2+} oxidation. Addition of NH_2GACl in the perovskite also helped optimize the energy levels of the perovskite and favorably adjusted it to the charge transport layers that resulted in faster charge carrier dynamics. Devices fabricated from NH_2GACl doped perovskites yielded a maximum PCE of 7.30% and were stable for more than 30 days when stored in nitrogen glove box. Very recently Kanatzidis and group reported a 9.61% efficient device by introducing 3-phenyl-2-propen-1-amine (PPA) in $FASnI_3$ perovskite [128]. The incorporation of these conjugated organic cations in the perovskite lattice resulted in larger grain sizes, reduced density of traps, enhanced charge extraction and increased overall structural stability of the perovskite film. Performance was optimized when the concentration of PPAI was kept at 15%. The champion cell yielded a V_{OC} of 0.56 V, J_{SC} of 23.34 $mA{\cdot}cm^{-2}$, FF of 73.5% and a PCE of 9.61% by reverse scan. Kanatzidis and group also demonstrated the large scale fabrication keeping the active area at 1 cm^2 to achieve a maximum PCE of 7.08%. When these devices were tested for stability it was revealed that the un-encapsulated 15% PPAI devices retained almost 92% of their initial performance even after 60 days, while being kept in nitrogen glove box. Song and group reported an 8.07% efficient device using a technique of secondary crystallization for improved film quality and remarkably reduced Sn^{2+} oxidation [129].

When stored in Nitrogen glove box, the un-encapsulated device retained 87% of its initial efficiency even after 1000 h.

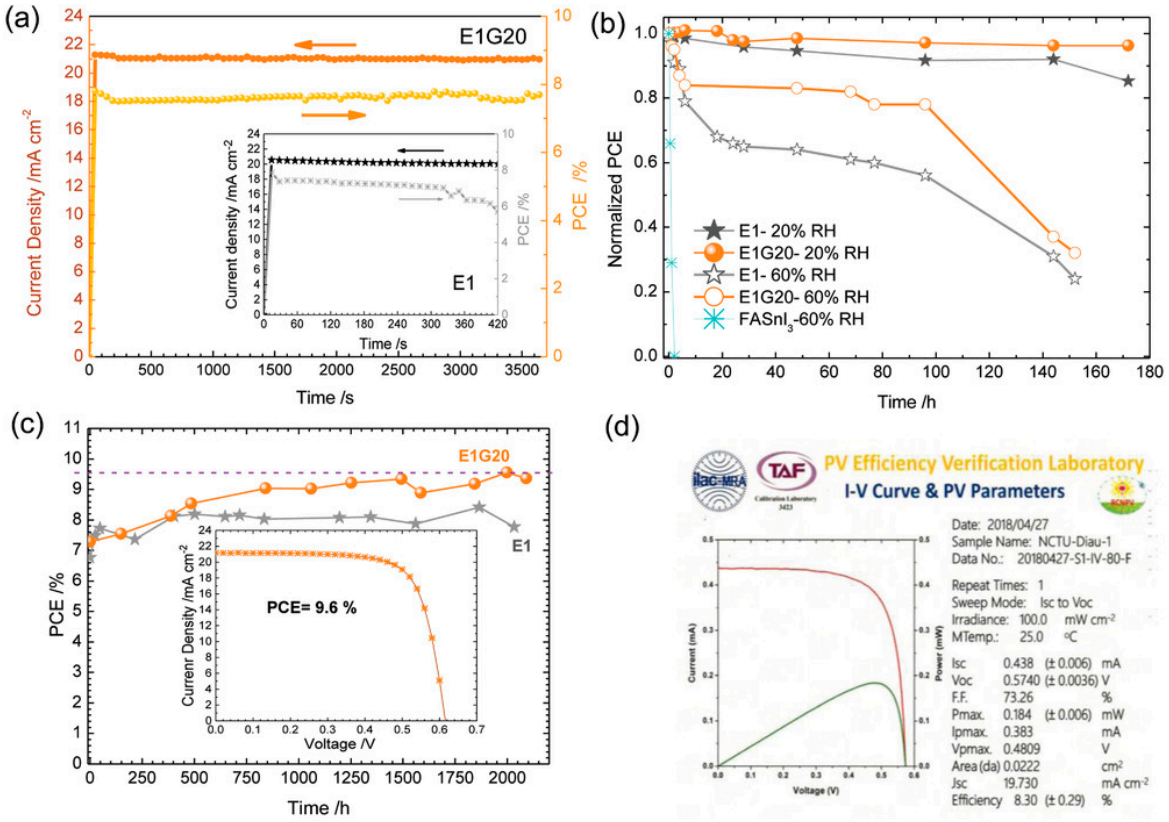

Figure 13. (**a**) Stabilized PCE and J_{SC} of E1G20 and E1 (shown in the inset) devices taken at the position of maximum power under 1 sun irradiation from AM1.5G solar simulator for 3600 s; PCE of both devices E1 and E1G20 as a function of storage period in two environments: (**b**) un-encapsulated devices in ambient air with RH = 20% and 60%, (**c**) Nitrogen glove box, and (**d**) certified efficiency 8.30% for the E1G20 device in an ISO-approved PV Efficiency Verification Laboratory in Taiwan. Adapted with permission from [124]. Copyright © 2018, WILEY-VCH Verlag GmbH & Co. KGaA, Weinheim.

Han et al. [130] reported a 10.81% efficient device by controlling $FASnI_3$ nucleation at solution-air interface. A tailor made organic cation, pentafluorophen-oxyethylammonium iodide (FOEI) was introduced in the perovskite lattice, which reduced the surface energy of solution-air surface and enhanced the crystallization intensity of perovskite films by 20-fold. PSCs fabricated from these films provided a long term stability of 500 h under continuous 1 sun illumination. A unique blend of Sn triple-halide amorphous layer and Cs-formamidinium tin iodide polycrystals was reported by Liu et al. [131] very recently to achieve PCE of over 10% with a 1000 h stability. An amorphous-polycrystalline perovskite film composed of a Sn triple-halide amorphous layer and $CsFASnI_3$ polycrystals was fabricated. The resulted structure proved very efficient in blocking moisture and oxygen resulting in elevated efficiency and enhanced stability. The champion device provided a PCE of 10.4% with a V_{OC} of 0.64 V, a J_{SC} of 21.6 mA·cm^{-2}, and FF of 75.2%. The encapsulated device maintained over 95% of its initial PCE for more than 1000 h. Jiang et al. [132] reported an unprecedented V_{OC} of 0.94 V for $PEA_xFA_{1-x}SnI_3$ based PSC, using indene-C_{60} bisadduct (ICBA) as ETL. The introduction of ICBA as ETL instead of commonly used PCBM considerably suppressed the iodide remote doping resulting in a higher V_{OC} and PCE. Champion device showed a PCE of 12.4% with shelf life of more than 3800 h.

Use of PEA^+ or $EADI_2$ is desirable to reduce trap density and enhance perovskite stability by improving crystal grain and orientation. However, doping optimized amount of Ge into the perovskite matrix is the latest focus of research [133,134]. The ab initio density functional theory (DFT) simulations performed on mixed elements Ca/(Ge, Sn) and Sr/(Ge, Sn) perovskites revealed that they have higher stability than Pb based perovskite deives [135]. Hayase and group introduced Ge in the perovskite lattice to significantly reduce trap density and suppress Sn vacancies. When 7.5% mol of Ge was added, the total trap density of the perovskite was doubly reduced to 4.14×10^{20} cm^{-3} and PCE of 7.45% was realized [136]. Because of the double positive effects of both PEA^+ and Ge^+ on the stability of the perovskite, the un-encapsulated device retained 70% of its PCE for 3 h under continuous 1 Sun illumination in ambient conditions.

To further increase the stability of mixed perovsite devices Chen et al. [134] replaced FA with Cs. Devices fabricated with $CsSn_{0.5}Ge_{0.5}I_3$ perovskties yielded a PCE of 7.11%. This perovskite had remarkable stability because of a stable native-oxide layer that formed on its surface when the perovskite got exposed to air. This stable native-oxide layer had completely encapsulated the surface of the perovskite which resulted in more than 500 h operational stability under continuous 1 Sun illumination in inert environment [134]. Although remarkably stable, these devices showed low PCE as compared to organic cation based perovskites. Very recently Hayase and group reported the most efficient Sn based PSC with a PCE of more than 13% [137]. To achieve such an outstanding PCE they used two different strategies of efficiency enhancement simultaneously. First of which involved the addition of metals to suppress Sn oxidation, while the second involved the addition of A cite cations to control perovskite crystallization. An optimized concentration of EAI was added to the perovskite lattice to favorably align energy bands between the perovskite and charge transport layers. To remove any iodide deficiency in the film GeI_2 doping was performed, which combined with EAI addition reduced the trap density of the perovskite by 1 order of magnitude. In addition by controlling the amount of EAI in the perovskite lattice the tolerance factor close to 1 was achieved. This proved that this method can be successfully used to produce considerably stable crystal structures.

When devices were fabricated from GeI_2 doped perovskite employing p-i-n architecture (FTO/PEDOT:PSS/GeI_2 doped Sn-perovskite/C_{60}/BCP/Ag/Au), PCE of 13.24% was achieved with a J_{SC} of 20.32 $mA{\cdot}cm^{-2}$, a V_{OC} of 0.84 V and a FF of 78% [137]. This is the highest value of PCE reported for Sn based perovskites till date. Table 7 show the progress in performance mixed cation devices has made so far. Tables 7 and 8 prove the importance of these devices in search of environment friendly highly efficient PSCs.

Table 7. Performance of best Mixed tin halide (s) based devices reported until 2020.

Year	Device Architecture	Perovskite Film Fabrication Technique/Perovskite Film	J_{SC} (mA·cm^{-2})	V_{OC} (V)	FF	EFF (%)	Ref.
2017	ITO/PEDOT:PSS/Perovskite/C_{60}/BCP/Ag	Spin Coating using DMSO as solvent + Annealing/$(FA)_x(MA)_{1-x}SnI_3$ + SnF_2	21.2	0.61	0.627	8.12	[107]
2017	FTO/c-TiO_2/mp-TiO_2-Perovskite/PTAA/Au	Spin Coating using DMF + DMSO as solvent + Annealing /{en}$FASnI_3$ + SnF_2	22.54	0.480	65.96	7.14	[110]
2017	FTO/c-TiO_2/mp-TiO_2-Perovskite/PTAA/Au	Spin Coating using DMF + DMSO as solvent + Annealing /{en}$MASnI_3$ + SnF_2	24.28	0.428	0.6372	6.63	[111]
2017	FTO/c-TiO_2/mp-TiO_2-Perovskite/PTAA/Au	Spin Coating using DMF + DMSO as solvent + Annealing /{en}$CsSnI_3$ + SnF_2	25.07	0.280	0.5382	3.79	[111]
2017	FTO/c-TiO_2/mp-TiO_2-Perovskite/PTAA/Au	Spin coating using DMSO as solvent/$(BA)_2(MA)_3Sn_4I_{13}$ + SnF_2 + triethylphosphine (TEP)	24.1	0.229	0.457	2.53	[115]
2017	ITO/NiO_x/Perovskite/PCBM/Al	Spin Coating using DMF + DMSO as solvent /$(PEA)_2(FA)_{n-1}Sn_nI_{3n+1}$+ SnF_2	14.44	0.59	0.69	5.94	[116]
2018	ITO/LiF/PEDOT:PSS/Perovskite/C_{60}/BCP/Ag	Multichannel interdiffusion two-step film fabrication protocol/$(PEA,FA)SnI_3$	20.07	0.47	0.74	6.98	[118]
2018	ITO/PEDOT:PSS/Perovskite/C_{60}/BCP/Al	Spin Coating using DMF + DMSO as solvent + Anti solvent dripping + Annealing/$(PEA)_2(FA)_{n-1}Sn_nI_{3n+1}$	24.1	0.525	0.71	9	[119]
2018	ITO/PEDOT:PSS/Perovskite/C_{60}/BCP/Ag	Spin Coating using DMSO as solvent+ Hot antisolvent treatment+Annealing in DMSO vapor atmoshpere/ $(FA)_x(MA)_{1-x}SnI_3$ + SnF_2	19.4	0.55	0.67	7.2	[110]
2018	ITO/PEDOT:PSS/Perovskite/C_{60}/BCP/Al	Spin Coating using DMF + DMSO as solvent + Antisolvent dripping / $FA_{0.75}MA_{0.25}SnI_3$ + SnF_2	24.3	0.55	0.673	9.06	[109]
2018	ITO/Perovskite/$PC_{61}BM$/BCP/Al	Spin Coating using DMF as solvent /Cs_xRb_{1-x} SnI_3 + Excess SnI_2	8.11 ± 0.53	0.48 ± 0.04	0.46 ± 0.05	1.81 ± 0.30	[120]
2018	ITO/PEDOT:PSS/Perovskite/C_{60}/BCP/Ag	Spin Coating +Annealing/$Cs_xFA_{1-x}FASnI_3$	20.70	0.44	0.668	6.08	[121]
2018	ITO/PEDOT:PSS/Perovskite/C_{60} /BCP/Ag	Spin Coating using DMSO as solvent + Antisolvent dripping/$FASnI_3$–$y$$EDAI_2$+$SnF_2$	21.3	0.538	0.718	8.9	[122]
2019	FTO/mp-TiO_2-Perovskite/BDT-4D/Au	Spin Coating using DMF + DMSO as solvent + Annealing /{en}$FASnI_3$ + SnF_2	22.41	0.497	0.682	7.59	[112]
2019	ITO/PEDOT:PSS/Perovskite/$PC_{60}BM$/Al	Spin Coating using DMF + DMSO as solvent + Antisolvent dripping/ $MA_{0.75}FA_{0.15}PEA_{0.1}Sn(Br_{0.25}I_{0.75})_3$	16.45	0.49	0.633	4.63	[123]
2019	ITO/PEDOT:PSS/Perovskite/C_{60} /BCP/Ag.	—/$GA_xFA_{1-x-2y}SnI_3$–$y$$EDAI_2$+$SnF_2$	21.2	0.619	0.729	9.6	[124]
2019	ITO/PEDOT:PSS/Perovskite/C_{60}/BCP/Ag	Spin Coating using DMSO as solvent + Antisolvent dripping + Annealing/ $PPA_xFA_{1-x}SnI_3$	23.34	0.56	0.735	9.61	[128]

Table 7. *Cont.*

Year	Device Architecture	Perovskite Film Fabrication Technique/Perovskite Film	J_{SC} ($mA \cdot cm^{-2}$)	V_{OC} (V)	FF	EFF (%)	Ref.
2020	ITO/PEDOT:PSS/ Perovskite/PCBM+PEI/Ag	Spin Coating using DMSO + DMF as solvent + Antisolvent dripping + Annealing/ $NH_2GACl+FASnI_3+SnF_2$	19.30 ± 0.35	0.54 ± 0.02	0.681 ± 0.084	7.10 ± 0.2	[127]
2020	FTO/c-TiO_2/mp-TiO_2/perovskite/PTAA/Au	$BA_2(FA)_{n-1}Sn_nI_{3n+1}$	22.02	0.439	0.433	4.12	[117]
2020	ITO/PEDOT:PSS/Perovskite/C_{60}/BCP/Ag	Secondary crystallization growth (SCG) technique/ $FA_{0.75}MA_{0.25}SnI_{2.75}Br_{0.25}$	22.3	0.52	0.695	8.07	[129]
2020	ITO/PEDOT:PSS/Perovskite/C_{60}/BCP/Ag	Spin Coating using DMSO as solvent + Antisolvent dripping of CB + Annealing/$FASnI_3$-FOEI	21.59	0.67	0.75	10.81	[130]
2020	ITO/PEDOT:PSS/Perovskite/ PCBM/BCP/Ag	Spin Coating using DMSO as solvent + Antisolvent dripping of CB + Annealing/$CsFASnI_3$	21.6	0.64	0.752	10.4	[131]
2020	ITO/PEDOT/Perovskite/ICBA/BCP/Ag	Spin Coating using DMSO + DMF as solvent + Antisolvent dripping of toluene + Annealing/ $PEA_xFA_{1-x}SnI_3$+SCN	17.4	0.94	0.75	12.4	[132]
2020	FTO/PEDOT:PSS/Perovskite/C_{60}/BCP/Ag/Au	Spin Coating using DMSO + DMF as solvent + Antisolvent dripping of CB + Annealing/$FA_{0.92}PEA_{0.08}Sn_xGe_{1-x}I_3$	21.92	0.46	0.73	7.45	[136]
2020	FTO/PEDOT:PSS/perovskite/C_{60}/BCP/Ag/Au.	GeI_2 doped $(FA_{0.9}EA_{0.1})_{0.98}EDA_{0.01}SnI_3$	20.32	0.84	0.78	13.24	[137]

Table 8. Stability of Mixed Cation tin halide(s) based perovskites.

Year	Device Architecture	Testing Environment	Stability	Ref.
2017	FTO/c-TiO_2/mp-TiO_2-$(BA)_2(MA)_3Sn_4I_{13}$ + SnF_2 + triethylphosphine (TEP)/PTAA/Au	Encapsulated devices under inert environment	Retained almost 90% of initial efficiency after 720 h	[115]
2017	ITO/PEDOT:PSS/$(FA)_x(MA)_{1-x}SnI_3$ + SnF_2/C_{60}/BCP/Ag	Encapsulated devices stored in inert environment	Retained almost 80% of initial efficiency after 400 h	[107]
2017	FTO/c-TiO_2/mp-TiO_2- {en}$FASnI_3$ + SnF_2/PTAA/Au	Encapsulated devices when stored	Retained almost all of their initial performance after 1000 h	[110]
2018	ITO/PEDOT:PSS/$FA_{0.75}MA_{0.25}SnI_3$ + SnF_2/C_{60}/BCP/Al	Encapsulated devices stored in inert environment	Retained almost 75% of their initial efficiencies after 720 h	[109]
2018	ITO/PEDOT:PSS/$Cs_xFA_{1-x}FASnI_3$/C_{60}/BCP/Ag	Encapsulated devices stored in inert environment	Remained stable for almost 2000 h	[121]
2018	ITO/PEDOT:PSS/$FASnI_3$–$y$$EDAI_2$+$SnF_2$/$C_{60}$/BCP/Ag	Encapsulated devices	Retained 90% of their initial efficiencies upto 2000 h	[122]
2019	ITO/PEDOT:PSS/ $GA_xFA_{1-x-2y}SnI_3$–$y$$EDAI_2$+$SnF_2$/$C_{60}$ /BCP/Ag.	Encapsulated device under 1 Sun illumination in ambient condition (RH = 50%) Un-encapsulated device stored in ambient condition (RH = 60%) Un-encapsulated device stored in ambient condition (RH = 20%)Un-encapsulated device stored in inert environment	Efficiency remained stable for 1 h Retained 80% of its initial PCE after 96 h Retained 100% of its initial PCE after 170 h PCE increased from 7.3% to 9.6% after 2000 h	[124]
2019	ITO/PEDOT:PSS/ $PPA_xFA_{1-x}SnI_3$/C_{60}/BCP/Ag	Un-encapsulated device stored in inert environment	Retained 90% of its initial PCE after 1440 h	[128]
2020	ITO/PEDOT:PSS/NH_2GACl+$FASnI_3$/PCBM+PEI/Ag	Un-encapsulated device stored in inert environment	Retained 90% of its initial PCE after 720 h	[127]
2020	FTO/c-TiO_2/mp-TiO_2/$BA_2(FA)_{n-1}Sn_nI_{3n+1}$/PTAA/Au	Un-encapsulated device stored in inert environment	Retained 80% of its initial PCE after 336 h	[117]
2020	ITO/PEDOT:PSS/$FA_{0.75}MA_{0.25}SnI_{2.75}Br_{0.25}$/$C_{60}$/ BCP/Ag	Un-encapsulated devices stored in inert environment	Retained 87% of their initial PCEs after 1000 h	[129]
2020	ITO/PEDOT:PSS/ $FASnI_3$-FOEI /C_{60}/BCP/Ag	Under continuous 1 Sun irradiation	Remained Stable for 500 h	[130]
2020	ITO/PEDOT:PSS/$CsFASnI_3$/ PCBM/BCP/Ag	Encapsulated device operation at simulated illumination of AM 1.5 G	Retained 95% of its initial PCE after 1000 h	[131]
2020	ITO/PEDOT / $PEA_xFA_{1-x}SnI_3$+SCN/ICBA/BCP/Ag	Encapsulated device stored in shelf	Retained 90% of its initial PCE for 3800 h	[132]
2020	FTO/PEDOT:PSS/$FA_{0.92}PEA_{0.08}Sn_xGe_{1-x}I_3$/$C_{60}$/BCP/Ag/Au	Un-encapsulated devices continuous operation at simulated illumination of AM 1.5 G in ambient conditions	Retained 70% of their initial PCEs for 3 h	[136].
2020	FTO/PCBM/$CsSn_{0.5}Ge_{0.5}I_3$-Native oxide/Spiro-OMeTAD/Au	Un-encapsulated devices continuous operation at simulated illumination of AM 1.5 G in inert conditions	Retained more than 90% of their initial PCEs for 500 h	[134]

6. Conclusions and Outlook

In this comprehensive Review, we have summarized all the efforts made on enhancing the performance and stability of Sn based PSCs from the very first report in 2014 to reports published in 2020. Performance and stability of Sn based PSCs is largely depended on perovskite film quality, device architecture and fabrication technique. Optimizing film deposition technique, interface modification and cation substitution have attracted much attention in recent years. Band gap engineering and solvent engineering proved effective in elevating overall PCE and stability of PSCs. Although still lagging in both efficiency and stability when compared to conventional Pb based perovskites, the Sn based counterparts are progressing ever so rapidly. With excellent optical and electrical properties and recent demonstration of efficiency exceeding 13 % the prospect of these perovskites playing a leading role in the future PV market cannot be ruled out. PCE can be significantly improved from the current highest reported efficiencies of 7.78 % [60], 10.17 % [81], 4.81 % [37,90] and 13.24% for $MASnX_3$, $FASnX_3$, $CsSnI_3$ and $MCSnX_3$, respectively. As the theoretical maximum PCE calculated for $MASnX_3$, $FASnX_3$ and $CsSnI_3$ based PSCs is 19.9%, 26.9%, and 25.6% respectively [37]. Based on our thorough analysis, we will provide suggestions on ways to further elevate the PCE and improve stability of tin-based PSCs. Moreover, focusing the commercial applications of Sn based PSCs in building integrated photovoltaics (BIPVs), suggestions to enhance transparency of PSCs are also provided.

- Minimizing oxygen exposure. One of the major reasons for low performance is Sn^{2+} oxidation. Reducing oxygen exposure during film growth by using techniques such as reducing vapor atmosphere [50] and vacuum growth [129] can significantly improve both efficiency and stability by minimizing p-type doping and enhancing film quality.
- Controlling perovskite crystallization. To reduce density of trap states and optimize charge carrier dynamics different strategies can be used such as introduction of [poly(ethylene-co-vinyl acetate) [82], pentafluorophen-oxyethylammonium iodide (FOEI) [130] or triethylphosphine (TEP) [115] in the perovskite matrix.
- Purification of Sn sources to prevent oxidation. Any commercial SnX_2 source contains Sn^{4+}, even those with 99 % purity contain a significant concentration of oxidized Sn^{4+} resulting in poor performance and reproducibility issues [80]. Addition of tin powder can solve this problem by reacting with Sn^{4+} and reducing it to Sn^{2+} state.
- Inverted p–i–n architecture should be preferred. Better quality of perovskite film can be formed on HTLs by avoiding using salt-doped hole selective layers (HSLs), known to damage Sn perovskite [51,70]. Also p-i-n architecture can favorably align the energy levels of HTL and ETL with perovskite than when used in conventional n-i-p configuration.
- Increasing V_{OC} by optimizing energy levels. While, the short circuit current (J_{SC}) of the PSCs is approaching the theoretical limit, the open circuit voltage (V_{OC}) emerges as a major limiting factor for overall performance of Sn based PSCs. V_{OC} is reduced greatly due to the existence of severe recombination and mismatched energy levels in the device. New techniques of bandgap engineering must be explored along trying more suitable materials as HTL and ETL. For example, Jiang et al. [132] used indene-C_{60} bisadduct (ICBA) as ETL instead of commonly used PCBM which considerably suppressed the iodide remote doping resulting in a record V_{OC} of 0.94 V and PCE of 12.4 % with shelf life of more than 3800 h.
- Regulating the A site cation to achieve a tolerance factor of nearly 1. An inverse relation exists between tolerance factor and lattice strain of perovskite crystal. Optimizing A site cation with proper substitution is vital to achieve high performance and stability. Regulating A cite cation can make the tolerance factor as close to one as possible, resulting in a stable perovskite structure. For example Nishimura et al. [137] partially substituted formamidinium cation with ethylammonium cation to achieve tolerance factor of 0.9985, achieving record PCE exceeding 13%.
- Doping Ge in Sn based PSCs. Ge is known to passivate traps and stabilize the mixed 2D/3D perovskite lattice by simultaneously suppressing defect/trap states and Sn^{2+} oxidation [133,134].

The addition of an optimum amount of Ge to develop efficient and stable tin-based PSCs should be an efficient approach. Ge^{2+} oxidizes into Ge^{4+} resulting in a thin GeO_4 protecting layer encapsulating tin perovskite crystals. The highest PCE of 13.24 % reported for Sn based PSCs is achieved doping Ge in the perovskite lattice [137].

- Enhancing transparency using bandgap engineering. Halides (Cl, Br, I) play a major role in determining the bandgap of the perovskite. As the halide radii decrease, the bandgap of perovskite increases, allowing more light in the visible region to pass through the perovskite film. For example, the optical bandgap changed from 1.27 eV for pure $CsSnI_3$ to 1.37 eV for $CsSnI_2Br$, and from 1.65 eV for $CsSnIBr_2$ to 1.75 eV for $CsSnBr_3$. The increasing bromine content also induced a change in the color of perovskite films from black to light brown, increasing transparency [88].
- Use of transparent contact. Currently most of the fabricated devices use relatively thick (~70 nm or more) metal film as back contact which makes the design opaque. However, a fully semitransparent PSC can be achieved by using 2D structures, transparent conducting oxides (TCOs), graphene electrodes and metal nanowires etc.

Recent progress in the field confirms that Sn based PSCs has great potential for commercialization with very optimistic future prospects. Starting with a PCE of 5.73 % and a shelf life of 12 h, within few years the PCE has exceeded 13% and stability reached 3800 h. With further research and resources directed in this field these nontoxic PSCs will be a major trend of the future.

Author Contributions: Writing-Original Draft Preparation, S.A.A.S., and Z.G.; Data Curation, M.H.S., K.K., K.G., F.S., J.S., A.K.T. and Y.G.; Writing-Review &Editing, Z.G. All authors have read and agreed to the published version of the manuscript.

Funding: This research was supported by Dongguan University of Technology.

Acknowledgments: The authors acknowledge the financial support provided by Dongguan University of Technology to carry out this extensive research work.

Conflicts of Interest: The authors declare no conflict of interest.

References

1. Green, M.A.; Hishikawa, Y.; Dunlop, E.D.; Levi, D.H.; Hohl-Ebinger, J.; Yoshita, M.; Ho-Baillie, A.W.Y. Solar cell efficiency tables (Version 53). *Prog. Photovolt. Res. Appl.* **2019**, *27*, 3–12. [CrossRef]
2. Lin, J.-T.; Hu, Y.-K.; Hou, C.-H.; Liao, C.-C.; Chuang, W.-T.; Chiu, C.-W.; Tsai, M.-K.; Shyue, J.-J.; Chou, P.-T. Superior Stability and Emission Quantum Yield (23% ± 3%) of Single-Layer 2D Tin Perovskite TEA2SnI4 via Thiocyanate Passivation. *Small* **2020**, *16*, 2000903. [CrossRef] [PubMed]
3. Gao, W.; Li, P.; Chen, J.; Ran, C.; Wu, Z. Interface Engineering in Tin Perovskite Solar Cells. *Adv. Mater. Interfaces* **2019**, *6*, 1901322. [CrossRef]
4. Mali, S.S.; Shim, C.S.; Hong, C.K. Highly porous Zinc Stannate (Zn_2SnO_4) nanofibers scaffold photoelectrodes for efficient methyl ammonium halide perovskite solar cells. *Sci. Rep.* **2015**, *5*, 11424. [CrossRef] [PubMed]
5. Mali, S.S.; Shim, C.S.; Hong, C.K. Highly stable and efficient solid-state solar cells based on methylammonium lead bromide ($CH_3NH_3PbBr_3$) perovskite quantum dots. *NPG Asia Mater.* **2015**, *7*, e208. [CrossRef]
6. Xie, F.; Chen, C.-C.; Wu, Y.; Li, X.; Cai, M.; Liu, X.; Yang, X.; Han, L. Vertical recrystallization for highly efficient and stable formamidinium-based inverted-structure perovskite solar cells. *Energy Environ. Sci.* **2017**, *10*, 1942–1949. [CrossRef]
7. Liu, T.; Zhou, Y.; Li, Z.; Zhang, L.; Ju, M.G.; Luo, D.; Yang, Y.; Yang, M.; Kim, D.H.; Yang, W. Stable Formamidinium-Based Perovskite Solar Cells via In Situ Grain Encapsulation. *Adv. Energy Mater.* **2018**, *8*, 1800232. [CrossRef]
8. Zhou, W.; Zhao, Y.; Zhou, X.; Fu, R.; Li, Q.; Zhao, Y.; Liu, K.; Yu, D.; Zhao, Q. Light-independent ionic transport in inorganic perovskite and ultrastable Cs-based perovskite solar cells. *J. Phys. Chem. Lett.* **2017**, *8*, 4122–4128. [CrossRef]
9. Liang, J.; Wang, C.; Wang, Y.; Xu, Z.; Lu, Z.; Ma, Y.; Zhu, H.; Hu, Y.; Xiao, C.; Yi, X. All-inorganic perovskite solar cells. *J. Am. Chem. Soc.* **2016**, *138*, 15829–15832. [CrossRef]

10. Qin, P.; Tanaka, S.; Ito, S.; Tetreault, N.; Manabe, K.; Nishino, H.; Nazeeruddin, M.K.; Grätzel, M. Inorganic hole conductor-based lead halide perovskite solar cells with 12.4% conversion efficiency. *Nat. Commun.* **2014**, *5*, 3834. [CrossRef]
11. Krishnamoorthy, T.; Ding, H.; Yan, C.; Leong, W.L.; Baikie, T.; Zhang, Z.; Sherburne, M.; Li, S.; Asta, M.; Mathews, N. Lead-free germanium iodide perovskite materials for photovoltaic applications. *J. Mater. Chem. A* **2015**, *3*, 23829–23832. [CrossRef]
12. Asghar, M.; Zhang, J.; Wang, H.; Lund, P. Device stability of perovskite solar cells—A review. *Renew. Sustain. Energy Rev.* **2017**, *77*, 131–146. [CrossRef]
13. Chondroudis, K.; Mitzi, D.B. Electroluminescence from an organic− inorganic perovskite incorporating a quaterthiophene dye within lead halide perovskite layers. *Chem. Mater.* **1999**, *11*, 3028–3030. [CrossRef]
14. Mitzi, D.B.; Chondroudis, K.; Kagan, C.R. Organic-inorganic electronics. *IBM J. Res. Dev.* **2001**, *45*, 29–45. [CrossRef]
15. Kojima, A.; Teshima, K.; Shirai, Y.; Miyasaka, T. Organometal halide perovskites as visible-light sensitizers for photovoltaic cells. *J. Am. Chem. Soc.* **2009**, *131*, 6050–6051. [CrossRef] [PubMed]
16. Im, J.-H.; Lee, C.-R.; Lee, J.-W.; Park, S.-W.; Park, N.-G. 6.5% efficient perovskite quantum-dot-sensitized solar cell. *Nanoscale* **2011**, *3*, 4088–4093. [CrossRef]
17. Kim, H.-S.; Lee, C.-R.; Im, J.-H.; Lee, K.-B.; Moehl, T.; Marchioro, A.; Moon, S.-J.; Humphry-Baker, R.; Yum, J.-H.; Moser, J.E. Lead iodide perovskite sensitized all-solid-state submicron thin film mesoscopic solar cell with efficiency exceeding 9%. *Sci. Rep.* **2012**, *2*, 591. [CrossRef]
18. Zhu, X. *The Perovskite Fever and Beyond*; ACS Publications: Washington, DC, USA, 2016.
19. Heo, J.H.; Im, S.H.; Noh, J.H.; Mandal, T.N.; Lim, C.-S.; Chang, J.A.; Lee, Y.H.; Kim, H.-j.; Sarkar, A.; Nazeeruddin, M.K. Efficient inorganic–organic hybrid heterojunction solar cells containing perovskite compound and polymeric hole conductors. *Nat. Photonics* **2013**, *7*, 486. [CrossRef]
20. Zhou, H.; Chen, Q.; Li, G.; Luo, S.; Song, T.-b.; Duan, H.-S.; Hong, Z.; You, J.; Liu, Y.; Yang, Y. Interface engineering of highly efficient perovskite solar cells. *Science* **2014**, *345*, 542–546. [CrossRef]
21. Park, J.H.; Seo, J.; Park, S.; Shin, S.S.; Kim, Y.C.; Jeon, N.J.; Shin, H.W.; Ahn, T.K.; Noh, J.H.; Yoon, S.C. Efficient CH3NH3PbI3 perovskite solar cells employing nanostructured p-type NiO electrode formed by a pulsed laser deposition. *Adv. Mater.* **2015**, *27*, 4013–4019. [CrossRef]
22. Dong, Q.; Yuan, Y.; Shao, Y.; Fang, Y.; Wang, Q.; Huang, J. Abnormal crystal growth in CH_3 NH_3 PbI_{3-x} Cl x using a multi-cycle solution coating process. *Energy Environ. Sci.* **2015**, *8*, 2464–2470. [CrossRef]
23. Carnie, M.J.; Charbonneau, C.; Davies, M.L.; Troughton, J.; Watson, T.M.; Wojciechowski, K.; Snaith, H.; Worsley, D.A. A one-step low temperature processing route for organolead halide perovskite solar cells. *Chem. Commun.* **2013**, *49*, 7893–7895. [CrossRef] [PubMed]
24. Zhao, Y.; Zhu, K. Solution Chem. engineering toward high-efficiency perovskite solar cells. *J. Phys. Chem. Lett.* **2014**, *5*, 4175–4186. [CrossRef] [PubMed]
25. Hao, F.; Stoumpos, C.C.; Liu, Z.; Chang, R.P.; Kanatzidis, M.G. Controllable perovskite crystallization at a gas–solid interface for hole conductor-free solar cells with steady power conversion efficiency over 10%. *J. Am. Chem. Soc.* **2014**, *136*, 16411–16419. [CrossRef]
26. Zhao, D.; Ke, W.; Grice, C.R.; Cimaroli, A.J.; Tan, X.; Yang, M.; Collins, R.W.; Zhang, H.; Zhu, K.; Yan, Y. Annealing-free efficient vacuum-deposited planar perovskite solar cells with evaporated fullerenes as electron-selective layers. *Nano Energy* **2016**, *19*, 88–97. [CrossRef]
27. Li, J.; Munir, R.; Fan, Y.; Niu, T.; Liu, Y.; Zhong, Y.; Yang, Z.; Tian, Y.; Liu, B.; Sun, J. Phase Transition Control for High-Performance Blade-Coated Perovskite Solar Cells. *Joule* **2018**, *2*, 1313–1330. [CrossRef]
28. Gribkova, O.L.; Kabanova, V.A.; Tameev, A.R.; Nekrasov, A.A. Ink-Jet Printing of Polyaniline Layers for Perovskite Solar Cells. *Tech. Phys. Lett.* **2019**, *45*, 858–861. [CrossRef]
29. Barrows, A.T.; Pearson, A.J.; Kwak, C.K.; Dunbar, A.D.; Buckley, A.R.; Lidzey, D.G. Efficient planar heterojunction mixed-halide perovskite solar cells deposited via spray-deposition. *Energy Environ. Sci.* **2014**, *7*, 2944–2950. [CrossRef]
30. Rong, Y.; Ming, Y.; Ji, W.; Li, D.; Mei, A.; Hu, Y.; Han, H. Toward Industrial-Scale Production of Perovskite Solar Cells: Screen Printing, Slot-Die Coating, and Emerging Techniques. *J. Phys. Chem. Lett.* **2018**, *9*, 2707–2713. [CrossRef]

31. Song, Z.; Watthage, S.C.; Phillips, A.B.; Heben, M.J. Pathways toward high-performance perovskite solar cells: Review of recent advances in organo-metal halide perovskites for photovoltaic applications. *J. Photonics Energy* **2016**, *6*, 022001. [CrossRef]
32. Green, M.A.; Dunlop, E.D.; Hohlebinger, J.; Yoshita, M.; Kopidakis, N.; Hobaillie, A. Solar cell efficiency tables (Version 55). *Prog. Photovolt.* **2020**, *28*, 3–15. [CrossRef]
33. Saliba, M.; Correa-Baena, J.-P.; Wolff, C.M.; Stolterfoht, M.; Phung, N.; Albrecht, S.; Neher, D.; Abate, A. How to Make over 20% Efficient Perovskite Solar Cells in Regular (n–i–p) and Inverted (p–i–n) Architectures. *Chem. Mater.* **2018**, *30*, 4193–4201. [CrossRef]
34. Abate, A. Perovskite solar cells go lead free. *Joule* **2017**, *1*, 659–664. [CrossRef]
35. Kopacic, I.; Friesenbichler, B.; Hoefler, S.F.; Kunert, B.; Plank, H.; Rath, T.; Trimmel, G. Enhanced Performance of Germanium Halide Perovskite Solar Cells through Compositional Engineering. *ACS Appl. Energy Mater.* **2018**, *1*, 343–347. [CrossRef]
36. Stoumpos, C.C.; Frazer, L.; Clark, D.J.; Kim, Y.S.; Rhim, S.H.; Freeman, A.J.; Ketterson, J.B.; Jang, J.I.; Kanatzidis, M.G. Hybrid Germanium Iodide Perovskite Semiconductors: Active Lone Pairs, Structural Distortions, Direct and Indirect Energy Gaps, and Strong Nonlinear Optical Properties. *J. Am. Chem. Soc.* **2015**, *137*, 6804–6819. [CrossRef]
37. Qian, J.; Xu, B.; Tian, W. A comprehensive theoretical study of halide perovskites ABX3. *Org. Electron.* **2016**, *37*, 61–73. [CrossRef]
38. Cortecchia, D.; Dewi, H.A.; Yin, J.; Bruno, A.; Chen, S.; Baikie, T.; Boix, P.P.; Grätzel, M.; Mhaisalkar, S.; Soci, C.; et al. Lead-Free MA2CuClxBr4–x Hybrid Perovskites. *Inorg. Chem.* **2016**, *55*, 1044–1052. [CrossRef]
39. Stoumpos, C.C.; Malliakas, C.D.; Kanatzidis, M.G. Semiconducting tin and lead iodide perovskites with organic cations: Phase transitions, high mobilities, and near-infrared photoluminescent properties. *Inorg. Chem.* **2013**, *52*, 9019–9038. [CrossRef]
40. Abdelaziz, S.; Zekry, A.; Shaker, A.; Abouelatta, M. Investigating the performance of formamidinium tin-based perovskite solar cell by SCAPS device simulation. *Opt. Mater.* **2020**, *101*, 109738. [CrossRef]
41. Takahashi, Y.; Hasegawa, H.; Takahashi, Y.; Inabe, T. Hall mobility in tin iodide perovskite CH3NH3SnI3: Evidence for a doped semiconductor. *J. Solid State Chem.* **2013**, *205*, 39–43. [CrossRef]
42. Noel, N.K.; Stranks, S.D.; Abate, A.; Wehrenfennig, C.; Guarnera, S.; Haghighirad, A.-A.; Sadhanala, A.; Eperon, G.E.; Pathak, S.K.; Johnston, M.B. Lead-free organic–inorganic tin halide perovskites for photovoltaic applications. *Energy Environ. Sci.* **2014**, *7*, 3061–3068. [CrossRef]
43. Stranks, S.D.; Eperon, G.E.; Grancini, G.; Menelaou, C.; Alcocer, M.J.; Leijtens, T.; Herz, L.M.; Petrozza, A.; Snaith, H.J. Electron-hole diffusion lengths exceeding 1 micrometer in an organometal trihalide perovskite absorber. *Science* **2013**, *342*, 341–344. [CrossRef] [PubMed]
44. Hao, F.; Stoumpos, C.C.; Cao, D.H.; Chang, R.P.; Kanatzidis, M.G. Lead-free solid-state organic–inorganic halide perovskite solar cells. *Nat. Photonics* **2014**, *8*, 489. [CrossRef]
45. Hao, F.; Stoumpos, C.C.; Guo, P.; Zhou, N.; Marks, T.J.; Chang, R.P.; Kanatzidis, M.G. Solvent-mediated crystallization of CH3NH3SnI3 films for heterojunction depleted perovskite solar cells. *J. Am. Chem. Soc.* **2015**, *137*, 11445–11452. [CrossRef] [PubMed]
46. Burschka, J.; Pellet, N.; Moon, S.-J.; Humphry-Baker, R.; Gao, P.; Nazeeruddin, M.K.; Grätzel, M. Sequential deposition as a route to high-performance perovskite-sensitized solar cells. *Nature* **2013**, *499*, 316. [CrossRef]
47. Zhang, S.; Audebert, P.; Wei, Y.; Al Choueiry, A.; Lanty, G.; Bréhier, A.; Galmiche, L.; Clavier, G.; Boissiere, C.; Lauret, J.-S. Preparations and characterizations of luminescent two dimensional organic-inorganic perovskite semiconductors. *Materials* **2010**, *3*, 3385–3406. [CrossRef]
48. Jeon, N.J.; Noh, J.H.; Kim, Y.C.; Yang, W.S.; Ryu, S.; Seok, S.I. Solvent engineering for high-performance inorganic–organic hybrid perovskite solar cells. *Nat. Mater.* **2014**, *13*, 897. [CrossRef]
49. Greul, E.; Docampo, P.; Bein, T. Synthesis of Hybrid Tin Halide Perovskite Solar Cells with Less Hazardous Solvents: Methanol and 1, 4-Dioxane. *Z. Für Anorg. Und Allg. Chem.* **2017**, *643*, 1704–1711. [CrossRef]
50. Song, T.-B.; Yokoyama, T.; Stoumpos, C.C.; Logsdon, J.; Cao, D.H.; Wasielewski, M.R.; Aramaki, S.; Kanatzidis, M.G. Importance of reducing vapor atmosphere in the fabrication of tin-based perovskite solar cells. *J. Am. Chem. Soc.* **2017**, *139*, 836–842. [CrossRef]
51. Yokoyama, T.; Cao, D.H.; Stoumpos, C.C.; Song, T.-B.; Sato, Y.; Aramaki, S.; Kanatzidis, M.G. Overcoming short-circuit in lead-free $CH_3NH_3SnI_3$ perovskite solar cells via kinetically controlled gas–solid reaction film fabrication process. *J. Phys. Chem. Lett.* **2016**, *7*, 776–782. [CrossRef]

52. Yokoyama, T.; Song, T.-B.; Cao, D.H.; Stoumpos, C.C.; Aramaki, S.; Kanatzidis, M.G. The origin of lower hole carrier concentration in methylammonium tin halide films grown by a vapor-assisted solution process. *ACS Energy Lett.* **2016**, *2*, 22–28. [CrossRef]
53. Weiss, M.; Horn, J.; Richter, C.; Schlettwein, D. Preparation and characterization of methylammonium tin iodide layers as photovoltaic absorbers. *Phys. Status Solidi* **2016**, *213*, 975–981. [CrossRef]
54. Hoshi, H.; Shigeeda, N.; Dai, T. Improved oxidation stability of tin iodide cubic perovskite treated by 5-ammonium valeric acid iodide. *Mater. Lett.* **2016**, *183*, 391–393. [CrossRef]
55. Fujihara, T.; Terakawa, S.; Matsushima, T.; Qin, C.; Yahiro, M.; Adachi, C. Fabrication of high coverage MASnI 3 perovskite films for stable, planar heterojunction solar cells. *J. Mater. Chem. C* **2017**, *5*, 1121–1127. [CrossRef]
56. Zhou, Y.; Zhang, T.; Li, C.; Liang, Z.; Gong, L.; Chen, J.; Xie, W.; Xu, J.; Liu, P. Rapid growth of high quality perovskite crystal by solvent mixing. *CrystEngComm* **2016**, *18*, 1184–1189. [CrossRef]
57. Handa, T.; Yamada, T.; Kubota, H.; Ise, S.; Miyamoto, Y.; Kanemitsu, Y. Photocarrier recombination and injection dynamics in long-term stable lead-free $CH_3NH_3SnI_3$ perovskite thin films and solar cells. *J. Phys. Chem. C* **2017**, *121*, 16158–16165. [CrossRef]
58. Ma, L.; Hao, F.; Stoumpos, C.C.; Phelan, B.T.; Wasielewski, M.R.; Kanatzidis, M.G. Carrier diffusion lengths of over 500 nm in lead-free perovskite $CH_3NH_3SnI_3$ films. *J. Am. Chem. Soc.* **2016**, *138*, 14750–14755. [CrossRef]
59. Tsai, C.M.; Mohanta, N.; Wang, C.Y.; Lin, Y.P.; Yang, Y.W.; Wang, C.L.; Hung, C.H.; Diau, E.W.G. Formation of Stable Tin Perovskites Co-crystallized with Three Halides for Carbon-Based Mesoscopic Lead-Free Perovskite Solar Cells. *Angew. Chem. Int. Ed.* **2017**, *56*, 13819–13823. [CrossRef]
60. Wang, P.; Li, F.; Jiang, K.; Zhang, Y.; Fan, H.; Zhang, Y.; Miao, Y.; Huang, J.; Gao, C.; Zhou, X. Ion Exchange/Insertion Reactions for Fabrication of Efficient Methylammonium Tin Iodide Perovskite Solar Cells. *Adv. Sci.* **2020**, 1903047. [CrossRef]
61. Yu, Y.; Zhao, D.; Grice, C.R.; Meng, W.; Wang, C.; Liao, W.; Cimaroli, A.J.; Zhang, H.; Zhu, K.; Yan, Y. Thermally evaporated methylammonium tin triiodide thin films for lead-free perovskite solar cell fabrication. *RSC Adv.* **2016**, *6*, 90248–90254. [CrossRef]
62. Peng, L.; Xie, W. Theoretical and experimental investigations on the bulk photovoltaic effect in lead-free perovskites MASnI3 and FASnI3. *RSC Adv.* **2020**, *10*, 14679–14688. [CrossRef]
63. Wang, F.; Ma, J.; Xie, F.; Li, L.; Chen, J.; Fan, J.; Zhao, N. Organic Cation-Dependent Degradation Mechanism of Organotin Halide Perovskites. *Adv. Funct. Mater.* **2016**, *26*, 3417–3423. [CrossRef]
64. Shi, T.; Zhang, H.-S.; Meng, W.; Teng, Q.; Liu, M.; Yang, X.; Yan, Y.; Yip, H.-L.; Zhao, Y.-J. Effects of organic cations on the defect physics of tin halide perovskites. *J. Mater. Chem. A* **2017**, *5*, 15124–15129. [CrossRef]
65. Baikie, T.; Fang, Y.; Kadro, J.M.; Schreyer, M.; Wei, F.; Mhaisalkar, S.G.; Graetzel, M.; White, T.J. Synthesis and crystal Chem. of the hybrid perovskite (CH_3 NH_3) PbI_3 for solid-state sensitised solar cell applications. *J. Mater. Chem. A* **2013**, *1*, 5628–5641. [CrossRef]
66. Amat, A.; Mosconi, E.; Ronca, E.; Quarti, C.; Umari, P.; Nazeeruddin, M.K.; Graätzel, M.; de Angelis, F. Cation-induced band-gap tuning in organohalide perovskites: Interplay of spin–orbit coupling and octahedra tilting. *Nano Lett.* **2014**, *14*, 3608–3616. [CrossRef]
67. Koh, T.M.; Krishnamoorthy, T.; Yantara, N.; Shi, C.; Leong, W.L.; Boix, P.P.; Grimsdale, A.C.; Mhaisalkar, S.G.; Mathews, N. Formamidinium tin-based perovskite with low E g for photovoltaic applications. *J. Mater. Chem. A* **2015**, *3*, 14996–15000. [CrossRef]
68. Lee, S.J.; Shin, S.S.; Kim, Y.C.; Kim, D.; Ahn, T.K.; Noh, J.H.; Seo, J.; Seok, S.I. Fabrication of efficient formamidinium tin iodide perovskite solar cells through SnF2–pyrazine complex. *J. Am. Chem. Soc.* **2016**, *138*, 3974–3977. [CrossRef] [PubMed]
69. Liao, W.; Zhao, D.; Yu, Y.; Grice, C.R.; Wang, C.; Cimaroli, A.J.; Schulz, P.; Meng, W.; Zhu, K.; Xiong, R.G. Lead-free inverted planar formamidinium tin triiodide perovskite solar cells achieving power conversion efficiencies up to 6.22%. *Adv. Mater.* **2016**, *28*, 9333–9340. [CrossRef] [PubMed]
70. Jung, M.-C.; Raga, S.R.; Qi, Y. Properties and solar cell applications of Pb-free perovskite films formed by vapor deposition. *RSC Adv.* **2016**, *6*, 2819–2825. [CrossRef]
71. Zeng, W.; Cui, D.; Li, Z.; Tang, Y.; Yu, X.; Li, Y.; Deng, Y.; Ye, R.; Niu, Q.; Xia, R. Surface optimization by poly(α-methylstyrene) as additive in the antisolution to enhance lead-free Sn-based perovskite solar cells. *Sol. Energy* **2019**, *194*, 272–278. [CrossRef]

72. Ke, W.; Stoumpos, C.C.; Logsdon, J.L.; Wasielewski, M.R.; Yan, Y.; Fang, G.; Kanatzidis, M.G. TiO2–ZnS cascade electron transport layer for efficient formamidinium tin iodide perovskite solar cells. *J. Am. Chem. Soc.* **2016**, *138*, 14998–15003. [CrossRef] [PubMed]
73. Xi, J.; Wu, Z.; Jiao, B.; Dong, H.; Ran, C.; Piao, C.; Lei, T.; Song, T.B.; Ke, W.; Yokoyama, T. Multichannel Interdiffusion Driven FASnI3 Film Formation Using Aqueous Hybrid Salt/Polymer Solutions toward Flexible Lead-Free Perovskite Solar Cells. *Adv. Mater.* **2017**, *29*, 1606964. [CrossRef] [PubMed]
74. Zhu, Z.; Chueh, C.C.; Li, N.; Mao, C.; Jen, A.K.Y. Realizing Efficient Lead-Free Formamidinium Tin Triiodide Perovskite Solar Cells via a Sequential Deposition Route. *Adv. Mater.* **2018**, *30*, 1703800. [CrossRef] [PubMed]
75. Hsu, C.; Geanangel, R. Synthesis and studies of trimethylamine adducts with tin (II) halides. *Inorg. Chem.* **1977**, *16*, 2529–2534. [CrossRef]
76. Noh, J.H.; Im, S.H.; Heo, J.H.; Mandal, T.N.; Seok, S.I. Chemical management for colorful, efficient, and stable inorganic–organic hybrid nanostructured solar cells. *Nano Lett.* **2013**, *13*, 1764–1769. [CrossRef] [PubMed]
77. Eperon, G.E.; Stranks, S.D.; Menelaou, C.; Johnston, M.B.; Herz, L.M.; Snaith, H.J. Formamidinium lead trihalide: A broadly tunable perovskite for efficient planar heterojunction solar cells. *Energy Environ. Sci.* **2014**, *7*, 982–988. [CrossRef]
78. Zhang, M.; Lyu, M.; Yun, J.-H.; Noori, M.; Zhou, X.; Cooling, N.A.; Wang, Q.; Yu, H.; Dastoor, P.C.; Wang, L. Low-temperature processed solar cells with formamidinium tin halide perovskite/fullerene heterojunctions. *Nano Res.* **2016**, *9*, 1570–1577. [CrossRef]
79. Lee, S.J.; Shin, S.S.; Im, J.; Ahn, T.K.; Noh, J.H.; Jeon, N.J.; Seok, S.I.; Seo, J. Reducing carrier density in formamidinium tin perovskites and its beneficial effects on stability and efficiency of perovskite solar cells. *ACS Energy Lett.* **2017**, *3*, 46–53. [CrossRef]
80. Gu, F.; Ye, S.; Zhao, Z.; Rao, H.; Liu, Z.; Bian, Z.; Huang, C. Improving Performance of Lead-Free Formamidinium Tin Triiodide Perovskite Solar Cells by Tin Source Purification. *Sol. RRL* **2018**, *2*, 1800136. [CrossRef]
81. Wu, T.; Liu, X.; He, X.; Wang, Y.; Meng, X.; Noda, T.; Yang, X.; Han, L. Efficient and stable tin-based perovskite solar cells by introducing π-conjugated Lewis base. *Sci.China-Chem.* **2020**, *63*, 107–115. [CrossRef]
82. Liu, G.; Liu, C.; Lin, Z.; Yang, J.; Huang, Z.; Tan, L.; Chen, Y. Regulated Crystallization of Efficient and Stable Tin-Based Perovskite Solar Cells via a Self-Sealing Polymer. *ACS Appl. Mater. Interfaces* **2020**, *12*, 14049–14056. [CrossRef]
83. Lee, B.; He, J.; Chang, R.P.; Kanatzidis, M.G. All-solid-state dye-sensitized solar cells with high efficiency. *Nature* **2012**, *485*, 486.
84. Chen, Z.; Wang, J.J.; Ren, Y.; Yu, C.; Shum, K. Schottky solar cells based on CsSnI3 thin-films. *Appl. Phys. Lett.* **2012**, *101*, 093901. [CrossRef]
85. Kumar, M.H.; Dharani, S.; Leong, W.L.; Boix, P.P.; Prabhakar, R.R.; Baikie, T.; Shi, C.; Ding, H.; Ramesh, R.; Asta, M. Lead-free halide perovskite solar cells with high photocurrents realized through vacancy modulation. *Adv. Mater.* **2014**, *26*, 7122–7127. [CrossRef]
86. Park, N.-G. Organometal perovskite light absorbers toward a 20% efficiency low-cost solid-state mesoscopic solar cell. *J. Phys. Chem. Lett.* **2013**, *4*, 2423–2429. [CrossRef]
87. Chung, I.; Song, J.-H.; Im, J.; Androulakis, J.; Malliakas, C.D.; Li, H.; Freeman, A.J.; Kenney, J.T.; Kanatzidis, M.G. CsSnI3: Semiconductor or metal? High electrical conductivity and strong near-infrared photoluminescence from a single material. High hole mobility and phase-transitions. *J. Am. Chem. Soc.* **2012**, *134*, 8579–8587. [CrossRef] [PubMed]
88. Sabba, D.; Mulmudi, H.K.; Prabhakar, R.R.; Krishnamoorthy, T.; Baikie, T.; Boix, P.P.; Mhaisalkar, S.; Mathews, N. Impact of anionic Br–substitution on open circuit voltage in lead free perovskite (CsSnI3-xBr x) solar cells. *J. Phys. Chem. C* **2015**, *119*, 1763–1767. [CrossRef]
89. Marshall, K.P.; Walton, R.I.; Hatton, R.A. Tin perovskite/fullerene planar layer photovoltaics: Improving the efficiency and stability of lead-free devices. *J. Mater. Chem. A* **2015**, *3*, 11631–11640. [CrossRef]
90. Song, T.-B.; Yokoyama, T.; Aramaki, S.; Kanatzidis, M.G. Performance enhancement of lead-free tin-based perovskite solar cells with reducing atmosphere-assisted dispersible additive. *ACS Energy Lett.* **2017**, *2*, 897–903. [CrossRef]
91. Marshall, K.; Walker, M.; Walton, R.; Hatton, R. Enhanced stability and efficiency in hole-transport-layer-free $CsSnI_3$ perovskite photovoltaics. *Nat. Energy* **2016**, *1*, 16178. [CrossRef]

92. Gupta, S.; Bendikov, T.; Hodes, G.; Cahen, D. $CsSnBr_3$, a lead-free halide perovskite for long-term solar cell application: Insights on SnF_2 addition. *ACS Energy Lett.* **2016**, *1*, 1028–1033. [CrossRef]
93. Moghe, D.; Wang, L.; Traverse, C.J.; Redoute, A.; Sponseller, M.; Brown, P.R.; Bulović, V.; Lunt, R.R. All vapor-deposited lead-free doped $CsSnBr_3$ planar solar cells. *Nano Energy* **2016**, *28*, 469–474. [CrossRef]
94. Song, T.-B.; Yokoyama, T.; Logsdon, J.; Wasielewski, M.R.; Aramaki, S.; Kanatzidis, M.G. Piperazine Suppresses Self-Doping in CsSnI3 Perovskite Solar Cells. *ACS Appl. Energy Mater.* **2018**, *1*, 4221–4226. [CrossRef]
95. Li, W.; Li, J.; Li, J.; Fan, J.; Mai, Y.; Wang, L. Addictive-assisted construction of all-inorganic CsSnIBr 2 mesoscopic perovskite solar cells with superior thermal stability up to 473 K. *J. Mater. Chem. A* **2016**, *4*, 17104–17110. [CrossRef]
96. Wang, N.; Zhou, Y.; Ju, M.G.; Garces, H.F.; Ding, T.; Pang, S.; Zeng, X.C.; Padture, N.P.; Sun, X.W. Heterojunction-Depleted Lead-Free Perovskite Solar Cells with Coarse-Grained B-γ-CsSnI3 Thin Films. *Adv. Energy Mater.* **2016**, *6*, 1601130. [CrossRef]
97. Chen, L.-J.; Lee, C.-R.; Chuang, Y.-J.; Wu, Z.-H.; Chen, C. Synthesis and optical properties of lead-free cesium tin halide perovskite quantum rods with high-performance solar cell application. *J. Phys. Chem. Lett.* **2016**, *7*, 5028–5035. [CrossRef]
98. Tan, L.; Wang, W.; Li, Q.; Luo, Z.; Zou, C.; Tang, M.; Zhang, L.; He, J.; Quan, Z. Colloidal syntheses of zero-dimensional Cs 4 SnX 6 (X= Br, I) nanocrystals with high emission efficiencies. *Chem. Commun.* **2020**, *56*, 387–390. [CrossRef]
99. Wang, A.; Guo, Y.; Muhammad, F.; Deng, Z. Controlled synthesis of lead-free cesium tin halide perovskite cubic nanocages with high stability. *Chem. Mater.* **2017**, *29*, 6493–6501. [CrossRef]
100. Qiu, X.; Cao, B.; Yuan, S.; Chen, X.; Qiu, Z.; Jiang, Y.; Ye, Q.; Wang, H.; Zeng, H.; Liu, J. From unstable CsSnI3 to air-stable Cs2SnI6: A lead-free perovskite solar cell light absorber with bandgap of 1.48 eV and high absorption coefficient. *Sol. Energy Mater. Sol. Cells* **2017**, *159*, 227–234. [CrossRef]
101. Zhang, T.; Li, H.; Ban, H.; Sun, Q.; Shen, Y.; Wang, M. Efficient CsSnI3-based inorganic perovskite solar cells based on a mesoscopic metal oxide framework via incorporating a donor element. *J. Mater. Chem.* **2020**, *8*, 4118–4124. [CrossRef]
102. Li, J.; Huang, J.; Zhao, A.; Li, Y.; Wei, M. An inorganic stable Sn-based perovskite film with regulated nucleation for solar cell application. *J. Mater. Chem. C* **2020**, *8*, 8840–8845. [CrossRef]
103. Namvar, M.J.; Abbaspour, F.M.H.; Rezaei, R.M.; Behjat, A.; Mirzaei, M. The effect of inserting combined Rubidium-Cesium cation on performance of perovkite solar cell FAMAPb (IBr) 3. *J. Res. Many Body Syst.* **2019**, *8*, 12–142.
104. Zhang, X.; Liu, H.; Wang, W.; Zhang, J.; Xu, B.; Karen, K.L.; Zheng, Y.; Liu, S.; Chen, S.; Wang, K. Hybrid Perovskite Light-Emitting Diodes Based on Perovskite Nanocrystals with Organic–Inorganic Mixed Cations. *Adv. Mater.* **2017**, *29*, 1606405. [CrossRef] [PubMed]
105. Sun, Y.; Peng, J.; Chen, Y.; Yao, Y.; Liang, Z. Triple-cation mixed-halide perovskites: Towards efficient, annealing-free and air-stable solar cells enabled by Pb (SCN) 2 additive. *Sci. Rep.* **2017**, *7*, 46193. [CrossRef] [PubMed]
106. Salado, M.; Kokal, R.K.; Calio, L.; Kazim, S.; Deepa, M.; Ahmad, S. Identifying the charge generation dynamics in Cs+-based triple cation mixed perovskite solar cells. *Phys. Chem. Chem. Phys.* **2017**, *19*, 22905–22914. [CrossRef] [PubMed]
107. Zhao, Z.; Gu, F.; Li, Y.; Sun, W.; Ye, S.; Rao, H.; Liu, Z.; Bian, Z.; Huang, C. Mixed-Organic-Cation Tin Iodide for Lead-Free Perovskite Solar Cells with an Efficiency of 8.12%. *Adv. Sci.* **2017**, *4*, 1700204. [CrossRef]
108. Liu, J.; Ozaki, M.; Yakumaru, S.; Handa, T.; Nishikubo, R.; Kanemitsu, Y.; Saeki, A.; Murata, Y.; Murdey, R.; Wakamiya, A. Lead-Free Solar Cells based on Tin Halide Perovskite Films with High Coverage and Improved Aggregation. *Angew. Chem. Int. Ed.* **2018**, *57*, 13221–13225. [CrossRef] [PubMed]
109. Liu, X.; Yan, K.; Tan, D.; Liang, X.; Zhang, H.; Huang, W. Solvent engineering improves efficiency of lead-free tin-based hybrid perovskite solar cells beyond 9%. *ACS Energy Lett.* **2018**, *3*, 2701–2707. [CrossRef]
110. Ke, W.; Stoumpos, C.C.; Zhu, M.; Mao, L.; Spanopoulos, I.; Liu, J.; Kontsevoi, O.Y.; Chen, M.; Sarma, D.; Zhang, Y. Enhanced photovoltaic performance and stability with a new type of hollow 3D perovskite {en} $FASnI_3$. *Sci. Adv.* **2017**, *3*, e1701293. [CrossRef]

111. Ke, W.; Stoumpos, C.C.; Spanopoulos, I.; Mao, L.; Chen, M.; Wasielewski, M.R.; Kanatzidis, M.G. Efficient lead-free solar cells based on hollow {en} MASnI3 perovskites. *J. Am. Chem. Soc.* **2017**, *139*, 14800–14806. [CrossRef]
112. Vegiraju, S.; Ke, W.; Priyanka, P.; Ni, J.; Wu, Y.C.; Spanopoulos, I.; Yau, S.L.; Marks, T.J.; Chen, M.; Kanatzidis, M.G. Benzodithiophene Hole-Transporting Mater. for Efficient Tin-Based Perovskite Solar Cells. *Adv. Funct. Mater.* **2019**, *29*, 1905393. [CrossRef]
113. Smith, I.C.; Hoke, E.T.; Solis-Ibarra, D.; McGehee, M.D.; Karunadasa, H.I. A layered hybrid perovskite solar-cell absorber with enhanced moisture stability. *Angew. Chem. Int. Ed.* **2014**, *53*, 11232–11235. [CrossRef] [PubMed]
114. Cao, D.H.; Stoumpos, C.C.; Farha, O.K.; Hupp, J.T.; Kanatzidis, M.G. 2D homologous perovskites as light-absorbing materials for solar cell applications. *J. Am. Chem. Soc.* **2015**, *137*, 7843–7850. [CrossRef] [PubMed]
115. Cao, D.H.; Stoumpos, C.C.; Yokoyama, T.; Logsdon, J.L.; Song, T.-B.; Farha, O.K.; Wasielewski, M.R.; Hupp, J.T.; Kanatzidis, M.G. Thin films and solar cells based on semiconducting two-dimensional ruddlesden–popper (CH3 (CH2) 3NH3) 2 (CH3NH3) n− 1Sn n I3 n+ 1 perovskites. *ACS Energy Lett.* **2017**, *2*, 982–990. [CrossRef]
116. Liao, Y.; Liu, H.; Zhou, W.; Yang, D.; Shang, Y.; Shi, Z.; Li, B.; Jiang, X.; Zhang, L.; Quan, L.N. Highly oriented low-dimensional tin halide perovskites with enhanced stability and photovoltaic performance. *J. Am. Chem. Soc.* **2017**, *139*, 6693–6699. [CrossRef] [PubMed]
117. Li, F.; Xie, Y.; Hu, Y.; Long, M.; Zhang, Y.; Xu, J.; Qin, M.; Lu, X.; Liu, M. Effects of Alkyl Chain Length on Crystal Growth and Oxidation Process of Two-Dimensional Tin Halide Perovskites. *ACS Energy Lett.* **2020**, *5*, 1422–1429. [CrossRef]
118. Ran, C.; Xi, J.; Gao, W.; Yuan, F.; Lei, T.; Jiao, B.; Hou, X.; Wu, Z. Bilateral interface engineering toward efficient 2D–3D bulk heterojunction tin halide lead-free perovskite solar cells. *ACS Energy Lett.* **2018**, *3*, 713–721. [CrossRef]
119. Shao, S.; Liu, J.; Portale, G.; Fang, H.H.; Blake, G.R.; ten Brink, G.H.; Koster, L.J.A.; Loi, M.A. Highly reproducible Sn-based hybrid perovskite solar cells with 9% efficiency. *Adv. Energy Mater.* **2018**, *8*, 1702019. [CrossRef]
120. Marshall, K.P.; Tao, S.; Walker, M.; Cook, D.S.; Lloyd-Hughes, J.; Varagnolo, S.; Wijesekara, A.; Walker, D.; Walton, R.I.; Hatton, R.A. Cs 1−x Rb x SnI 3 light harvesting semiconductors for perovskite photovoltaics. *Mater. Chem. Front.* **2018**, *2*, 1515–1522. [CrossRef]
121. Gao, W.; Ran, C.; Li, J.; Dong, H.; Jiao, B.; Zhang, L.; Lan, X.; Hou, X.; Wu, Z. Robust Stability of Efficient Lead-Free Formamidinium Tin Iodide Perovskite Solar Cells Realized by Structural Regulation. *J. Phys. Chem. Lett.* **2018**, *9*, 6999–7006. [CrossRef]
122. Jokar, E.; Chien, C.-H.; Fathi, A.; Rameez, M.; Chang, Y.-H.; Diau, E.W.-G. Slow surface passivation and crystal relaxation with additives to improve device performance and durability for tin-based perovskite solar cells. *Energy Environ. Sci.* **2018**, *11*, 2353–2362. [CrossRef]
123. Weber, S.; Rath, T.; Kunert, B.; Resel, R.; Dimopoulos, T.; Trimmel, G. Dependence of material properties and photovoltaic performance of triple cation tin perovskites on the iodide to bromide ratio. *Mon. Fur Chem.* **2019**, *150*, 1921–1927. [CrossRef]
124. Jokar, E.; Chien, C.H.; Tsai, C.M.; Fathi, A.; Diau, E.W.G. Robust Tin-Based Perovskite Solar Cells with Hybrid Organic Cations to Attain Efficiency Approaching 10%. *Adv. Mater.* **2019**, *31*, 1804835. [CrossRef] [PubMed]
125. Kieslich, G.; Sun, S.; Cheetham, A.K. An extended tolerance factor approach for organic–inorganic perovskites. *Chem. Sci.* **2015**, *6*, 3430–3433. [CrossRef] [PubMed]
126. Stoumpos, C.C.; Mao, L.; Malliakas, C.D.; Kanatzidis, M.G. Structure–band gap relationships in hexagonal polytypes and low-dimensional structures of hybrid tin iodide perovskites. *Inorg. Chem.* **2016**, *56*, 56–73. [CrossRef]
127. Fu, Q.; Tang, X.; Li, D.; Huang, L.; Xiao, S.; Chen, Y.; Hu, T. An efficient and stable tin-based perovskite solar cell passivated by aminoguanidine hydrochloride. *J. Mater. Chem. C* **2020**, *8*, 7786–7792. [CrossRef]
128. Ran, C.; Gao, W.; Li, J.; Xi, J.; Li, L.; Dai, J.; Yang, Y.; Gao, X.; Dong, H.; Jiao, B. Conjugated Organic Cations Enable Efficient Self-Healing $FASnI_3$ Solar Cells. *Joule* **2019**, *3*, 3072–3087. [CrossRef]
129. Jin, Z.; Yu, B.-B.; Liao, M.; Liu, D.; Xiu, J.; Zhang, Z.; Lifshitz, E.; Tang, J.; Song, H.; He, Z. Enhanced efficiency and stability in Sn-based perovskite solar cells with secondary crystallization growth. *J. Energy Chem.* **2021**, *54*, 414–421. [CrossRef]

130. Meng, X.; Wang, Y.; Lin, J.; Liu, X.; He, X.; Barbaud, J.; Wu, T.; Noda, T.; Yang, X.; Han, L. Surface-Controlled Oriented Growth of FASnI3 Crystals for Efficient Lead-free Perovskite Solar Cells. *Joule* **2020**, *4*, 902–912. [CrossRef]
131. Liu, X.; Wang, Y.; Wu, T.; He, X.; Meng, X.; Barbaud, J.; Chen, H.; Segawa, H.; Yang, X.; Han, L. Efficient and stable tin perovskite solar cells enabled by amorphous-polycrystalline structure. *Nat. Commun.* **2020**, *11*, 2678. [CrossRef]
132. Jiang, X.; Wang, F.; Wei, Q.; Li, H.; Shang, Y.; Zhou, W.; Wang, C.; Cheng, P.; Chen, Q.; Chen, L. Ultra-high open-circuit voltage of tin perovskite solar cells via an electron transporting layer design. *Nat. Commun.* **2020**, *11*, 1245. [CrossRef] [PubMed]
133. Hayase, S.; Ito, N.; Kamarudin, M.A.K.; Shen, Q.; Ogomi, Y.; Iikubo, S.; Yoshino, K.; Minemoto, T.; Toyoda, T. Pb free perovskite solar cells consisting of mixed metal SnGe perovskite as light absorber. In Proceedings of the Conference Presentation SPIE, San Diego, CA, USA, 18 September 2018.
134. Chen, M.; Ju, M.-G.; Garces, H.F.; Carl, A.D.; Ono, L.K.; Hawash, Z.; Zhang, Y.; Shen, T.; Qi, Y.; Grimm, R.L.; et al. Highly stable and efficient all-inorganic lead-free perovskite solar cells with native-oxide passivation. *Nat. Commun.* **2019**, *10*, 16. [CrossRef] [PubMed]
135. Ali, R.; Hou, G.; Zhu, Z.; Yan, Q.; Zheng, Q.; Su, G. Stable mixed group II (Ca, Sr) and XIV (Ge, Sn) lead-free perovskite solar cells. *J. Mater. Chem.* **2018**, *6*, 9220–9227. [CrossRef]
136. Ng, C.H.; Hamada, K.; Kapil, G.; Kamarudin, M.A.; Wang, Z.; Iikubo, S.; Shen, Q.; Yoshino, K.; Minemoto, T.; Hayase, S. Reducing trap density and carrier concentration by a Ge additive for an efficient quasi 2D/3D perovskite solar cell. *J. Mater. Chem. A* **2020**, *8*, 2962–2968. [CrossRef]
137. Nishimura, K.; Kamarudin, M.A.; Hirotani, D.; Hamada, K.; Shen, Q.; Iikubo, S.; Minemoto, T.; Yoshino, K.; Hayase, S. Lead-free tin-halide perovskite solar cells with 13% efficiency. *Nano Energy* **2020**, *74*, 104858. [CrossRef]